Decadal Trends in the Oceanic Storage of Anthropogenic Carbon from 1994 to 2014

Jens Daniel Müller[1] (0000-0003-3137-0883), N. Gruber[1] (0000-0002-2085-2310), B. Carter[2,3] (0000-0003-2445-0711), R. Feely[3] (0000-0003-3245-3568), M. Ishii[4] (0000-0002-7328-4599), N. Lange[5], S.K. Lauvset[6] (0000-0001-8498-4067), A. Murata[7] (0000-0002-5931-2784), A. Olsen[8] (0000-0003-1696-9142), F.F. Pérez[9,10] (0000-0003-4836-8974), C. Sabine[12] (0000-0001-6945-8552), T. Tanhua[5] 0000-0002-0313-2557, R. Wanninkhof[13] (0000-0003-1973-3514), D. Zhu[1] (0000-0002-6033-9079)

[1]Environmental Physics, Institute of Biogeochemistry and Pollutant Dynamics, ETH Zurich, Zurich, Switzerland.

[2]Cooperative Institute for Climate, Ocean, and Ecosystem Studies, University of Washington, Seattle, WA, 98105.

[3]Pacific Marine Environmental Laboratory, National Oceanic and Atmospheric Administration, Seattle, WA, 98115.

[4]Meteorological Research Institute, Japan Meteorological Agency, Tsukuba, Japan.

[5]GEOMAR Helmholtz Centre for Ocean Research Kiel, Kiel, Germany.

[6]NORCE Norwegian Research Centre, Bjerknes Centre for Climate Research, Bergen, Norway.

[7]Japan Agency for Marine-Earth Science and Technology, Yokosuka, Kanagawa, 237-0061, Japan.

[8]Geophysical Institute, University of Bergen and Bjerknes Centre for Climate Research, Bergen, Norway.

[9]Instituto de Investigaciones Marinas (IIM), CSIC, Vigo, Spain.

[10]Oceans Department, Stanford University, Stanford, CA 94305, USA.

[12]University of Hawaii at Manoa, Honolulu, HI, 96822.

[13]Atlantic Oceanographic and Meteorological Laboratory, National Oceanographic and Atmospheric Administration, Miami, USA.

Corresponding author: Jens Daniel Müller (jensdaniel.mueller@usys.ethz.ch)

Key Points:

- The global ocean storage of anthropogenic carbon grew by 29 ± 3 and 27 ± 3 Pg C dec^{-1} from 1994 to 2004 and 2004 to 2014, respectively.
- The change in oceanic storage of anthropogenic carbon relative to the atmospheric CO_2 growth decreased by 15 ± 11% from the first to the second decade.
- This reduction is attributed to a decrease of the ocean buffer capacity and changes in ocean circulation.

Abstract

The oceanic uptake and resulting storage of the anthropogenic CO_2 (C_{ant}) that humans have emitted into the atmosphere moderates climate change. Yet our knowledge about how this uptake and storage has progressed in time remained limited. Here, we determine decadal trends in the storage of C_{ant} by applying the eMLR(C*) regression method to ocean interior observations collected repeatedly since the 1990s. We find that the global ocean storage of C_{ant} grew from 1994 to 2004 by 29 ± 3 Pg C dec^{-1} and from 2004 to 2014 by 27 ± 3 Pg C dec^{-1} (±1σ). The storage change in the second decade is about 15 ± 11% lower than one would expect from the first decade and assuming proportional increase with atmospheric CO_2. We attribute this reduction in sensitivity to a decrease of the ocean buffer capacity and changes in ocean circulation. In the Atlantic Ocean, the maximum storage rate shifted from the Northern to the Southern Hemisphere, plausibly caused by a weaker formation rate of North Atlantic Deep Waters and an intensified ventilation of mode and intermediate waters in the Southern Hemisphere. Our estimates of the C_{ant} accumulation differ from cumulative net air-sea flux estimates by several Pg C dec^{-1}, suggesting a substantial and variable, but uncertain net loss of natural carbon from the ocean. This indicates a considerable vulnerability of the ocean carbon sink to climate variability and change.

Plain language summary

The ocean takes up about 30% of the anthropogenic CO_2 that is emitted to the atmosphere by human activities. The removal of this anthropogenic CO_2 from the atmosphere counteracts climate change. The rate at which the ocean takes up anthropogenic CO_2 is controlled by its transport from the surface to the depth of the ocean, where most of it accumulates. Thus, we can quantify and understand the oceanic uptake by keeping track of the accumulation of

anthropogenic CO_2 in the ocean interior. In this study, we use a global collection of measurements of CO_2 in seawater to infer the temporal evolution of this accumulation between 1994 and 2014. We find that the ocean continued to act as a strong sink for CO_2 over this period, removing, on average, nearly 30 billion tons of carbon per decade. However, we also detect a possible weakening of this uptake, since the accumulation of anthropogenic CO_2 during the second decade was not as large as expected from the increase in atmospheric CO_2. Our findings suggest that the ocean sink for CO_2 might further shrink as climate change progresses.

1 Introduction

As a consequence of climate change, the ocean is warming, acidifying, becoming more stratified, and experiencing increasing winds and an intensified hydrological cycle (Cheng et al., 2022; IPCC, 2019; Jiang et al., 2019; Li et al., 2020; Young & Ribal, 2019). While the ocean itself has been vital to mitigate climate change over the past two centuries through its removal of CO_2 from the atmosphere (DeVries, 2014; Gruber et al., 2023; Khatiwala et al., 2009), a key concern is whether the ocean carbon sink will maintain its function in a changing climate. Models and observation-based estimates agree that since the beginning of the industrial period, the ocean has taken up roughly 30% of the total human CO_2 emissions due to fossil fuel combustion, cement production, and land use change (Crisp et al., 2022; Friedlingstein et al., 2022; Gruber et al., 2019; Khatiwala et al., 2009, 2013; Sabine et al., 2004). The observations from the first global survey of CO_2 in the ocean interior during the 1980s and 1990s (Key et al., 2004; Wallace, 1995) provided an important pillar for this consensus, demonstrating that between ~1800 and 1994, the ocean had taken up 118 ± 19 petagrams (10^{15}g) of anthropogenic carbon from the atmosphere (Sabine et al., 2004). Anthropogenic carbon (C_{ant}) refers to the additional carbon present in the ocean-atmosphere-land system due to human CO_2 emissions to the atmosphere (Gruber et al., 2023). We denote temporal changes in the ocean interior content of C_{ant} as ΔC_{ant}.

Another pillar supporting the consensus about the strength of the oceanic C_{ant} sink was established when the observational data were extended with the ocean interior measurements gathered during the second cycle of the repeat hydrography program in the framework of GO-SHIP, the Global Ocean Ship-based Hydrographic Investigations Program (Talley et al., 2016). Applying a modified version of the extended Multiple Linear Regression method (eMLR(C*)) to the data available until the early 2010s, Gruber et al. (2019) demonstrated that the ocean took up an additional 34 ± 4 Pg C of C_{ant} from 1994 to 2007 corresponding to a mean decadal storage rate of 26 ± 3 Pg C dec^{-1}. This globally integrated storage rate is indistinguishable from the growth that one would predict from the total C_{ant} storage in 1994 and assuming an increase of this inventory proportional with the rise in atmospheric CO_2. Hence, this finding suggested that up to 2007, the globally integrated oceanic C_{ant} sink had been responding in near steady-state fashion to the anthropogenic perturbation, without showing any discernible impact of climate change.

However, a first indication of a deviation from this proportional steady-state accumulation emerged in the spatial patterns of the reconstructed changes in C_{ant} storage between 1994 and 2007 (Gruber et al., 2019). By comparing these changes with those expected on the basis of the reconstructed storage of C_{ant} for 1994 (Sabine et al., 2004), Gruber et al (2019) found a roughly 20% decrease of the storage rate in the North Atlantic compensated by an increased storage rate in the South Atlantic. However, the robustness of these shifts remains unclear, because they were derived from the comparison of results from two different methodological approaches, both with poorly characterised uncertainties at the regional scale.

A second indication of a deviation from the proportional steady-state uptake emerged from the analysis of the difference between the ocean interior storage changes of C_{ant} and the net air-sea fluxes of CO_2 determined based on sea surface observations of pCO_2 (Landschützer et al., 2016). These surface flux estimates include the transfer of both anthropogenic CO_2 and natural CO_2 across the air-sea interface, with the latter referring to the carbon that was already present in the Earth System in preindustrial times (Gruber et al., 2023). The difference between storage and net fluxes amounted to 5 ± 3 Pg C over the 1994–2007 period and was interpreted as a non-steady state (i.e., climate-driven) outgassing of natural CO_2 from the ocean.

While some studies suggested that the outgassing of natural CO_2 may contribute to a long-term saturation of the oceanic carbon sink (Le Quéré et al., 2007), recent surface flux estimates actually indicate that the net global ocean carbon sink increased strongly over the past decade (Fay et al., 2021; Friedlingstein et al., 2022). But for reasons not yet fully understood, Global Ocean Biogeochemical Models (GOBMs) tend to suggest a smaller increase in uptake since around 2002 compared to the estimates based on the surface ocean pCO_2 observations (Hauck et al., 2019, Friedlingstein et al., 2022). Hence, the discrepancy between these two methods increased over the 2010s, culminating in the surface flux products estimating a 0.6 Pg C yr^{-1} stronger sink than the GOBMs for the 2010s (Friedlingstein et al., 2022). This discrepancy forces the authors of the Global Carbon Budget (GCB) to assign only a medium confidence level to the ocean sink estimate, as it represents the mean of the GOBMs and the surface flux products (Friedlingstein et al., 2022). Thus, independent information about the oceanic uptake of CO_2 by extending the knowledge about the oceanic accumulation of C_{ant} beyond 2007 would be very useful to help resolving this

discrepancy and to better understand the drivers for the changes in the strength of the ocean carbon sink.

Some independent information about the evolution of the ocean sink beyond 2007 is already available from regional analyses of the accumulation of C_{ant} over the last few decades. In the Pacific Ocean the C_{ant} inventory change was found to have increased from 8.8 ± 1.1 Pg C dec^{-1} between 1995 and 2005 to 11.7 ± 1.1 Pg C dec^{-1} between 2005 and 2015 (Carter et al., 2019). Even more pronounced increases were reported for the North Atlantic Ocean with an intensification of the C_{ant} storage from 1.9 ± 0.4 Pg C dec^{-1} for the 1989–2003 period to 4.4 ± 0.9 Pg C dec^{-1} from 2003 to 2014 (Woosley et al., 2016; Wanninkhof et al., 2010). While Woosley et al. (2016) reported a rather steady uptake behaviour in the South Atlantic, Gao et al. (2022) found that the rates of C_{ant} storage accelerated from the 1990s to the 2000s. In all regional studies, the temporal variability of the C_{ant} storage was attributed to changing ventilation patterns of the upper ocean. However, differences in time periods and statistical methods applied in the regional studies limit their synoptic assessment and prevent combining them into a global reconstruction of the oceanic increase in C_{ant} storage since 2007.

Such an extension of the reconstruction of the global increase in C_{ant} storage beyond 2007 is the key aim of this study. Our work profits from including ~100,000 additional observations of dissolved inorganic carbon (DIC) and related biogeochemical variables collected over the 2010s, which were compiled, quality-controlled, and made available by GLODAP, the Global Ocean Data Analysis Project (Lauvset et al., 2021). By consistently determining the storage increase between 1994 and 2004, and between 2004 and 2014, and benefitting from the reconstructed storage of C_{ant} for 1994, we can investigate for the first time the temporal evolution of the global increase in the oceanic storage of C_{ant}. This permits us to address whether the ocean has maintained its vital sink function in a changing climate. Our global-scale reconstruction of the oceanic storage of C_{ant} further serves as an important independent reference point for the ocean carbon sink estimates established by other means, especially in the context of the GCB (Friedlingstein et al., 2022) and the Intergovernmental Panel on Climate Change (IPCC) (Canadell et al., 2021).

2 Material and Methods

2.1 Overview of the Approach

Our global-scale analysis of the changes in the content of C_{ant} (ΔC_{ant}) is based on measurements of the dissolved inorganic carbon (DIC) content and related hydrographical and biogeochemical properties gathered from 1989–2020 and synthesised in the data product GLODAPv2.2021 (Olsen et al., 2016; Lauvset et al., 2021). This data product includes high-quality measurements from reoccupied sections for the purposes of diagnosing long term climate signals such as the accumulation of C_{ant}. The majority of the data used in this study stem from the JGOFS/WOCE global CO_2 survey conducted in the 1980s and 1990s (Key et al., 2004; Wallace, 1995), the repeat hydrography program GO-SHIP that began in 2003 and is now completing its second cycle (Sloyan et al., 2019; Talley et al., 2016), as well as a number of additional programs, including INDIGO, SAVE, TTO, JOIS, and GEOSECS (Key et al., 2004, and references therein). In addition to DIC, our analysis requires observations of salinity (S), temperature (T), total alkalinity (TA), oxygen (O_2), the apparent oxygen utilisation (AOU), silicate ($Si(OH)_4$), nitrate (NO_3^-), and phosphate (PO_4^{3-}). To extract the ΔC_{ant} signal from these data, we use the eMLR(C*) method (Clement & Gruber, 2018; Gruber et al., 2019) with a few modifications (see details below and in supplement S2).

Our application of the eMLR(C*) method employs the following steps:

1. The semi-conservative tracer C* (Gruber et al., 1996; Gruber & Sarmiento, 2002) is calculated from DIC as $C^* = DIC - 117\times[PO_4^{3-}] - 0.5\times(TA + 16\times[PO_4^{3-}])$. This conversion from DIC to C* removes a substantial part of the inorganic carbon variability that is due to ocean interior redistributions and biogeochemical transformations of natural carbon.
2. The observations are clustered in neutral density slabs (supplement S2.1) and ocean regions (Fig. S1), and assigned to one of the three sampling periods 1989–1999, 2000–2009, or 2010–2020 (Fig. 1).
3. Within each sampling period, the observed C* is adjusted to the respective reference year (t_{ref}) 1994, 2004, or 2014 assuming a transient steady state increase of C_{ant} (Gammon et al., 1982).
4. Within each neutral density slab and ocean region, a set of multiple linear regression

(MLR) models are fitted with $C^*(t_{ref})$ as target variable and all possible combinations of at least 2 out of the 7 considered predictor variables S, T, O_2, AOU, $Si(OH)_4$, NO_3^-, PO_4^{3-}.

5. The 10 best common MLR models for two compared sampling periods are selected within each density slab and ocean region based on the summed root mean squared error (RMSE), after excluding MLRs with strong multicollinearity between the predictors (supplement S2.2).
6. The decadal change in anthropogenic carbon is computed as the difference between the average C* distribution for each sampling period, i.e. $\Delta C_{ant} = C^*(t_{ref,n+1},) - C^*(t_{ref,n})$, where the C* distributions are predicted ("mapped") for each t_{ref} by applying the selected MLRs to a common set of predictor climatologies.
7. In surface waters, ΔC_{ant} is predicted based on an transient equilibrium approach (McNeil et al., 2003), which assumes that the increase of the surface ocean pCO_2 follows that of the atmosphere closely. This approach aims to avoid biases introduced by the seasonal and interannual variability of C* and the predictor variables.

The most important differences we introduced relative to the methods described by Clement and Gruber (2018) and Gruber et al. (2019) are detailed in section 2.3 and include a more thorough selection of the predictor variables and MLR models, a more robust and standardised quantification of uncertainties, and an assessment of structural reconstruction uncertainties through tests with synthetic data, which were performed in parallel to the analysis of the real-world observations. Our reconstruction of ΔC_{ant} with the eMLR(C*) method involves a number of choices regarding the configuration of the method. In sections 2.2 and 2.3 we describe the standard configuration that we use to derive the results we report as our best informed estimates. In section 2.4, we describe a number of reasonable alternative configurations. We use the offsets between results obtained with these plausible alternatives and the standard configuration as a basis for determining the uncertainty.

2.2 Data

This study relies on ocean interior observations of DIC, TA, S, T, O_2, $Si(OH)_4$, NO_3^-, and PO_4^{3-} collected in the global ocean from 1989 through 2020 (Fig. 1) and provided through GLODAPv2.2021 (Lauvset et al., 2021; Olsen et al., 2016). The apparent oxygen utilisation was calculated from oxygen, salinity, and conservative temperature (Graham & McDougall,

2013) according to the solubility from Weiss (1970) and used as an additional predictor variable. Observations were filtered based on the GLODAP flagging scheme, using only highest-quality data identified as those with a f-flag value of 2, which indicates acceptable, measured data according to a simplified version of the WOCE flagging scheme, and a qc-flag value of 1, which indicates adjusted or unadjusted data that have undergone GLODAP's full secondary quality control. With a few exceptions, only samples were included for which all required variables fulfil the strictest quality criteria. We deviated from this only for cases where our tests of the eMLR(C*) method with synthetic data (see supplement S4) revealed that omitting observations because of only one missing variable increased the biases of the ΔC_{ant} reconstructions. In these cases either data that did not fulfil the strictest quality criteria were included (7609 samples, 3.7% of all samples), or missing data were filled (7305 samples, 3.5%) using CANYON-B (Bittig et al., 2018) predictions (see supplement S1.3). In total, we used 206'836 samples for our standard case reconstruction.

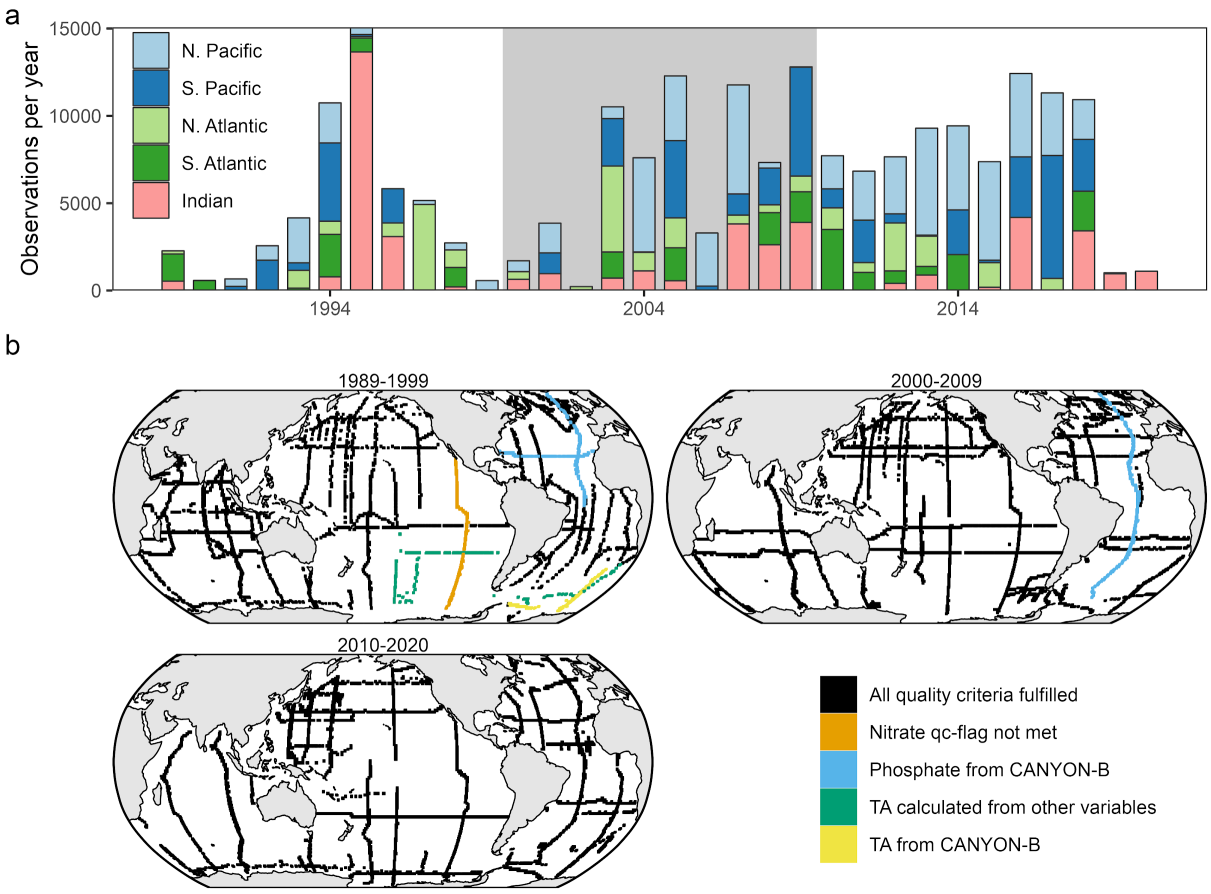

Fig. 1: Spatio-temporal coverage of observations from 1989–2020 as provided through GLODAPv2.2021 and after applying our flagging criteria. (a) Number of observations per year, where colours distinguish sampling regions according to the basin mask definition "5" in Fig. S1. The

shaded background indicates the assigned sampling periods 1989–1999 ($t_{ref,1}$ = 1994), 2000–2009 ($t_{ref,2}$ = 2004), and 2010–2020 ($t_{ref,3}$ = 2014). (b) Map of observations as used in our standard case for the three sampling periods. Cruises that fulfilled all flagging criteria are displayed in black, while cruises for which one parameter did not fulfil all criteria but were still included (see also Table S1) are highlighted in colour.

Although the GLODAP data have already undergone a secondary quality control and are — if required — adjusted to improve their internal consistency, we applied a number of additional adjustments to the DIC, TA, and phosphate observations. These data adjustments are supported by multiple independent lines of evidence and quantified based either on our decade-by-decade reanalysis of deep water crossovers originally determined by GLODAP, or on previously unaccounted offsets in the measurements of certified reference materials (CRM) for DIC and TA (see supplement S1.2 for details). This affected the majority of the DIC and TA measurements from the Indian Ocean in the 1990s (12843 samples, 6.2% of all samples), and the DIC, TA, and phosphate measurements in the North Pacific from the 2010s (35395 samples, 17.2% of all samples). Our proposed adjustments of the Indian Ocean data were formally accepted by GLODAP and applied in the release of GLODAPv2.2022 (Lauvset et al., 2022). In contrast, the proposed adjustments for the North Pacific are still under discussion by the GLODAP community, and while well justified, currently need to be viewed as preliminary. We thus discuss the relevance of the North Pacific adjustments for our results and conclusions in detail. The magnitude of these additional adjustments are generally small (<2 µmol kg^{-1} for DIC, <4 µmol kg^{-1} for TA, and <1% for phosphate) and below the adjustment limits normally considered by GLODAP. Still, these adjustments proved to be critical in our work, since an offset of 1 µmol kg^{-1} in DIC integrated over 3000 m amounts to a column inventory offset of ~3 mol m^{-2}, which is of similar magnitude as some of the decadal changes we are aiming to detect.

For the purpose of predicting the C* distributions, we used the objectively analysed climatology for the 1981 – 2010 period for salinity and temperature from the World Ocean Atlas 2018 (Locarnini et al., 2019; Zweng et al., 2019), in combination with phosphate, nitrate, silicate and oxygen from the global interior ocean mapped climatology based on GLODAPv2 (Lauvset et al., 2016). The climatological distribution of AOU was calculated in accordance with the observational data. For atmospheric CO_2 ($CO_{2,atm}$) data we use the globally averaged marine surface annual mean data provided by NOAA/GML (Lan et al.,

2022).

2.3 Standard configuration of the eMLR(C*) method

In the following, we describe the main changes of the eMLR(C*) method in comparison to the previous analysis by Gruber et al. (2019). Further minor configuration changes are presented in supplement S2.

2.3.1 Temporal clustering and C* adjustment to reference year

For the temporal clustering of the data, we assigned each observation to one of the following three sampling periods (start and end years included):

1989–1999 ($t_{ref,1}$ = 1994)
2000–2009 ($t_{ref,2}$ = 2004)
2010–2020 ($t_{ref,3}$ = 2014)

with the assigned reference years (t_{ref}) given in parenthesis.

Based on these three sampling periods, we estimated the C_{ant} storage changes between the reference years 1994–2004 and 2004–2014 (Fig. 1). The ΔC_{ant} estimates represent the changes over exactly ten years, from mid-year of the first to mid-year of the second reference year. In addition, we determined ΔC_{ant} directly for the twenty year period 1994–2014.

The adjustment of C* from the time of sample collection (t) to the reference year (t_{ref}) was calculated as $C^*(t_{ref}) = C^*(t) - \delta(t) * C_{ant}(t_{ref})$, with $\delta(t) = \Delta CO_{2,atm}(t\text{-}t_{ref}) / \Delta CO_{2,atm}(t_{ref}\text{-}t_{pi})$, where t_{pi} indicates preindustrial times (~1800) and $\Delta CO_{2,atm}$ is the change in atmospheric CO_2. We estimated the C_{ant} content in the reference year ($C_{ant}(t_{ref})$), by adding a proportional fraction of the reconstructed increase in C_{ant} over 13 years between 1994–2007 (ΔC_{ant}(1994–2007), Gruber et al., 2019) to the reconstructed C_{ant} in 1994 (C_{ant}(1994), Sabine et al., 2004), i.e., $\Delta C_{ant}(1994\text{–}t_{ref}) = (t_{ref}\text{-}1994) * \Delta C_{ant}(1994\text{–}2007) / 13$ years.

2.3.2 Spatial clustering and subsetting

For the fitting of the MLR models and mapping of ΔC_{ant} in the standard configuration, we clustered the observations and predictor climatologies horizontally into the Atlantic, Pacific

and Indian Ocean, according to mask "3" of our basin mask definitions (Fig. S1). To assess the contribution of the impact of this choice on the uncertainty of the reconstructed changes in C_{ant}, we investigated five other basin configurations (Fig. S1). For clustering in the vertical dimension, we used the same neutral density levels as employed by Gruber et al. (2019). Surface water samples collected shallower than 100 m were excluded from the MLR fitting to avoid seasonally biased observations.

2.3.3 Mapping C* and ΔC_{ant}

The spatial distribution of C* was mapped by predicting the best MLR models of each reference year with climatological distributions of the predictor variables. For this purpose, the ten best MLR models within each spatial cluster were selected as those with the lowest summed RMSE for the two paired sampling periods following Clement and Gruber (2018). The ten individually mapped C* distributions were then averaged and subtracted to derive the mean ΔC_{ant} distribution. In contrast to prior applications of the method, we included negative mapped ΔC_{ant} values, since (i) ΔC_{ant} can regionally be negative when water with low C_{ant} displaces water with high C_{ant}, (ii) setting negative values to zero could lead to positively biased ΔC_{ant} inventories, and (iii) our tests with synthetic data revealed a tendency to lower biases when negative values were retained.

2.3.4 Surface equilibrium ΔC_{ant}

In the standard configuration, the equilibrium ΔC_{ant} distribution at the sea surface was computed based on a rearranged definition of the Revelle factor, γ, as $\Delta C_{ant,eq}(t_{ref,n}–t_{ref,n+1}) = 1/\gamma \times DIC/pCO_2 \times \Delta CO_{2,atm}(t_{ref,n+1}-t_{ref,n})$, where DIC, pCO_2 and γ are the climatological surface values (Lauvset et al., 2016) adjusted to the mean $CO_{2,atm}$ of each analysis period. This adjustment of the climatological surface CO_2-system parameters to the mean $CO_{2,atm}$ was achieved by calculating as a first step the surface pCO_2 in 2002 based on the climatological values for temperature, salinity, DIC and TA, which are normalised to the same year (Lauvset et al., 2016). In a second step, the surface ocean pCO_2 was shifted according to the change in $CO_{2,atm}$, and DIC and γ were recalculated based on the new surface pCO_2. Thus, our surface equilibrium approach takes changes in the surface ocean buffer capacity into consideration. All CO_2-system calculations were done with the R-package seacarb (Gattuso et al., 2021) using the CO_2 dissociation constants from Lueker et al. (2000), the fluoride association constant from Perez and Fraga (1987) or Dickson & Riley (1979) at temperatures below 9°C and the acidity constant of hydrogen sulphide from Dickson (1990). To assess the

uncertainties associated with this equilibrium ΔC_{ant} estimate, we also used an independent observation-based estimate of the increase in surface DIC (Gregor & Gruber, 2021).

While previous studies defined a distinct depth and neutral density threshold to separate water masses for which the surface equilibrium or eMLR(C*) reconstructions are used to determine ΔC_{ant}, we blend both estimates smoothly over the top 200 m. For this purpose, the equilibrium ΔC_{ant} is calculated at the sea surface only, while the eMLR-based ΔC_{ant} is initially mapped across the entire water column. In a post processing step, the surface- and eMLR-based ΔC_{ant} estimates are averaged proportionally according to the water depth across the upper 200 m (e.g., 75% surface-based and 25% eMLR(C*)-based estimate at 50 m water depth).

2.4 Computation of global ΔC_{ant} inventories and sensitivities

Column inventories and inventories of ΔC_{ant} in this study represent integrals across the upper 3000 m of the water column. ΔC_{ant} reconstructions below 3000 m are not included in integrals to avoid the imprint of ΔC_{ant} uncertainties that are small in terms of amount content but considerable in terms of integrated inventory changes. Instead, we follow previous studies and account for C_{ant} storage changes below 3000 m by adding 2% to our global ΔC_{ant} inventories. This deep ocean scaling represents the fraction of the total C_{ant} inventory in 1994 beneath 3000 m according to Sabine et al. (2004). We further scale our global inventories for the storage of C_{ant} in unmapped regions according to previously determined fractions of the global C_{ant} storage that occurs in these regions, namely 2% in the Arctic Ocean (Tanhua et al., 2009), 1.5% in the Mediterranean Sea (Palmiéri et al., 2015), 1% in the Nordic Seas (Olsen et al., 2010), and 0.3% in the Sea of Japan (Park et al., 2006). In sum, the upscaling amounts to 7% of our directly mapped global ΔC_{ant} inventory. Regional inventories refer to the integral of directly mapped ΔC_{ant} distributions and no areal scaling was applied, e.g., the regional inventory of the Atlantic Ocean does not account for storage in the Mediterranean Sea. Thus, our global inventory differs from the sum of the regional inventories by 7%.

To relate the global decadal change in the oceanic C_{ant} inventory ($Inv(\Delta C_{ant})$) to the primary driver of the C_{ant} uptake, i.e., the increase in atmospheric CO_2 over the same decade ($\Delta CO_{2,atm}$), we compute the storage sensitivity $\beta = Inv(\Delta C_{ant}) / \Delta CO_{2,atm}$. Globally, the sensitivity β measures how much additional anthropogenic carbon the ocean takes up and

stores (Gruber et al., 2023; Ríos et al., 2012) in response to the increase in atmospheric CO_2. As long as atmospheric CO_2 increases close to exponentially, as was the case for the past 50 years, the sensitivity β is expected to remain constant, provided that ocean circulation remains in steady-state (Keeling, 1979) and ocean chemistry does not change. This implies that under these circumstances, changes in the oceanic storage of C_{ant} scale linearly with changes in atmospheric CO_2, i.e., $Inv(\Delta C_{ant}) = \beta * \Delta CO_{2,atm}$ (Gruber et al., 2023). Conversely, deviations from this linear scaling indicate changes in ocean circulation or other changes affecting β, such as the reduction in the oceanic buffering capacity owing to ongoing ocean acidification. Note, however, that this metric will be less useful when the atmospheric CO_2 growth rates will start to fall (see Gruber et al. (2023) for discussion).

For our regional and basin-scale analyses, we will use the regional expression of this sensitivity, i.e., the area-normalised storage sensitivity β_{area}, to achieve direct comparability of the storage sensitivity across different regions. It is defined as $\beta_{area} = \beta/A$, where A is the surface area of the region under consideration.

2.5 Determination of uncertainty and method testing

The most important sources of uncertainty associated with the eMLR(C*) method are structural in nature and involve choices associated with the configuration of the method (Clement and Gruber, 2018, Gruber et al., 2019). We identified the following six configuration choices as critical (1) the regional clustering of the data, (2) the approach to perform data adjustments, (3) the nutrient used to compute the target variable C*, (4) the approach to estimate surface ocean ΔC_{ant}, (5) the gap-filling of flagged data, and (6) the choice of predictor climatologies. In addition, we consider (7) an uncertainty contribution in our global ΔC_{ant} inventories arising from the scaling to account for C_{ant} storage changes in unmapped waters.

To assess the impact of these choices and to obtain an estimate of uncertainty of our reconstructions, we have reconstructed a set of total 10 alternative estimates of ΔC_{ant} using modified choices for each of the six configurations listed above. These modifications of the eMLR(C*) configuration are described in detail in supplement S4. We base our estimate of uncertainty on the ΔC_{ant} offsets between the standard case and the reconstructions obtained with the configuration changes. The individual offsets are considered as independent uncertainty contributions and combined as the square root of the sum of the squares (RSS) to

derive the standard uncertainty ($\pm 1\sigma$) of our reconstructions, which we consider as a 68% confidence interval. Throughout the results and discussion, we report all results together with this $\pm 1\sigma$ uncertainty. In figures, we display also the expanded $\pm 2\sigma$ uncertainty representing a confidence interval of 95%. For each variable that is derived from a primary ΔC_{ant} estimate (e.g., the decadal difference between two ΔC_{ant} estimates, the ocean-borne fraction, etc.) we combine individual uncertainties through standard error propagation.

In order to independently assess the quality of our ΔC_{ant} reconstructions against a known truth, we use synthetic data generated from the global ocean biogeochemical model (GOBM) CESM-ETHZ (Doney et al., 2009; Hauck et al., 2020; Yang et al., 2017) following the approach of (Clement & Gruber, 2018). The GOBM is a hindcast model forced with reanalysed atmospheric data and the observed atmospheric CO_2 trajectory. The synthetic data set was generated by subsetting the model output in space and time according to availability of real-world observations. The eMLR(C*) approach is then applied to the synthetic data set to reconstruct ΔC_{ant}. The comparison of the reconstructed ΔC_{ant} to the known model truth allows us to determine the biases of the reconstruction. Details and results of this assessment are given in the supplement S5.

In order to assess the sensitivity of our reconstructions to other sources of uncertainty, such as the limited sampling of the spatio-temporal variability of the changes in DIC, we performed additional eMLR(C*) analyses, wherein we pushed the configurations beyond the limits of what we consider a reasonable modification. For example, we limited the observations to those from repeatedly occupied sections, used other DIC variants than C* as target variable and omitted the data adjustments (see section 4.2). In contrast, other choices associated with the application of the eMLR(C*) method have shown to be of minor relevance for the uncertainty of the reconstructed ΔC_{ant} and were thus not considered in the uncertainty assessment (supplement S2). This applies, for example, to the choice of the a priori C_{ant} estimate used for the adjustment of C* to the reference year (Clement & Gruber, 2018).

3 Results

3.1 Column inventories

The storage changes in anthropogenic carbon (ΔC_{ant}) integrated over the upper 3000 m

(referred to as column inventories) reveal strong similarities during both decades of our analysis, i.e., between 1994 and 2004, and between 2004 and 2014 (Fig. 2a,b). The ΔC_{ant} column inventories vary markedly with latitude. The highest mean decadal C_{ant} storage changes of about 10 mol m^{-2} dec^{-1} located near the centre of the subtropical gyres (30–40° N/S) are about twice as high as those in the equatorial regions (10° N/S) and in the Southern Ocean south of 60°S. In the Southern Hemisphere, the consistently high ΔC_{ant} column inventories in all subtropical gyres form a circumpolar band, while in the Northern Hemisphere the storage changes per unit area in the Atlantic exceed those in the Pacific roughly by a factor of two. The general patterns of our ΔC_{ant} reconstructions are reminiscent of those reconstructed for the pre-industrial to 1994 period (Sabine et al., 2004) and for the 1994 to 2007 period (Gruber et al., 2019), supporting in first approximation the expectation of a steady-state increase in the oceanic storage of C_{ant}. We also note that our ΔC_{ant} column inventory reconstructions for the 1994–2007 period (Fig. S6) confirm those reported by Gruber et al. (2019) for the same period, supporting the consistency of our approaches and estimates despite the modifications of the eMLR(C*) method and our use of an updated database.

While the general pattern of the increases in the C_{ant} column inventories are similar in the two decades, there are distinct differences (Fig. 2c). These decadal differences are most pronounced in the Atlantic Ocean, where we find a shift of the highest ΔC_{ant} column inventories from the Northern to the Southern Hemisphere. In the subtropical latitudes (20–50 °N) of the North Atlantic, the mean, area-weighted ΔC_{ant} column inventory in the second decade is 3.7 ± 0.8 mol m^{-2} dec^{-1} lower compared to the first one (1994–2004: 12.1 ± 0.5; 2004–2014: 8.4 ± 0.6 mol m^{-2} dec^{-1}; ±1σ uncertainty). In contrast, the mean ΔC_{ant} column inventory in the subtropical latitudes of the South Atlantic (20–50 °S) is 4.7 ± 2.2 mol m^{-2} dec^{-1} higher in the second decade (1994–2004: 8.5 ± 0.9; 2004–2014: 13.2 ± 1.9 mol m^{-2} dec^{-1}). In other regions of the ocean, the decadal differences are within or close to the bounds of the uncertainty of our estimates inferred from a set of alternative reconstructions. We thus refrain from further analysis. Overall, the spatial patterns in the decadal difference of our ΔC_{ant} column inventories are reminiscent of the anomaly structure that Gruber et al. (2019) derived from a comparison of their ΔC_{ant} column inventories to the steady-state projection of the total C_{ant} inventory in 1994 from Sabine et al. (2004).

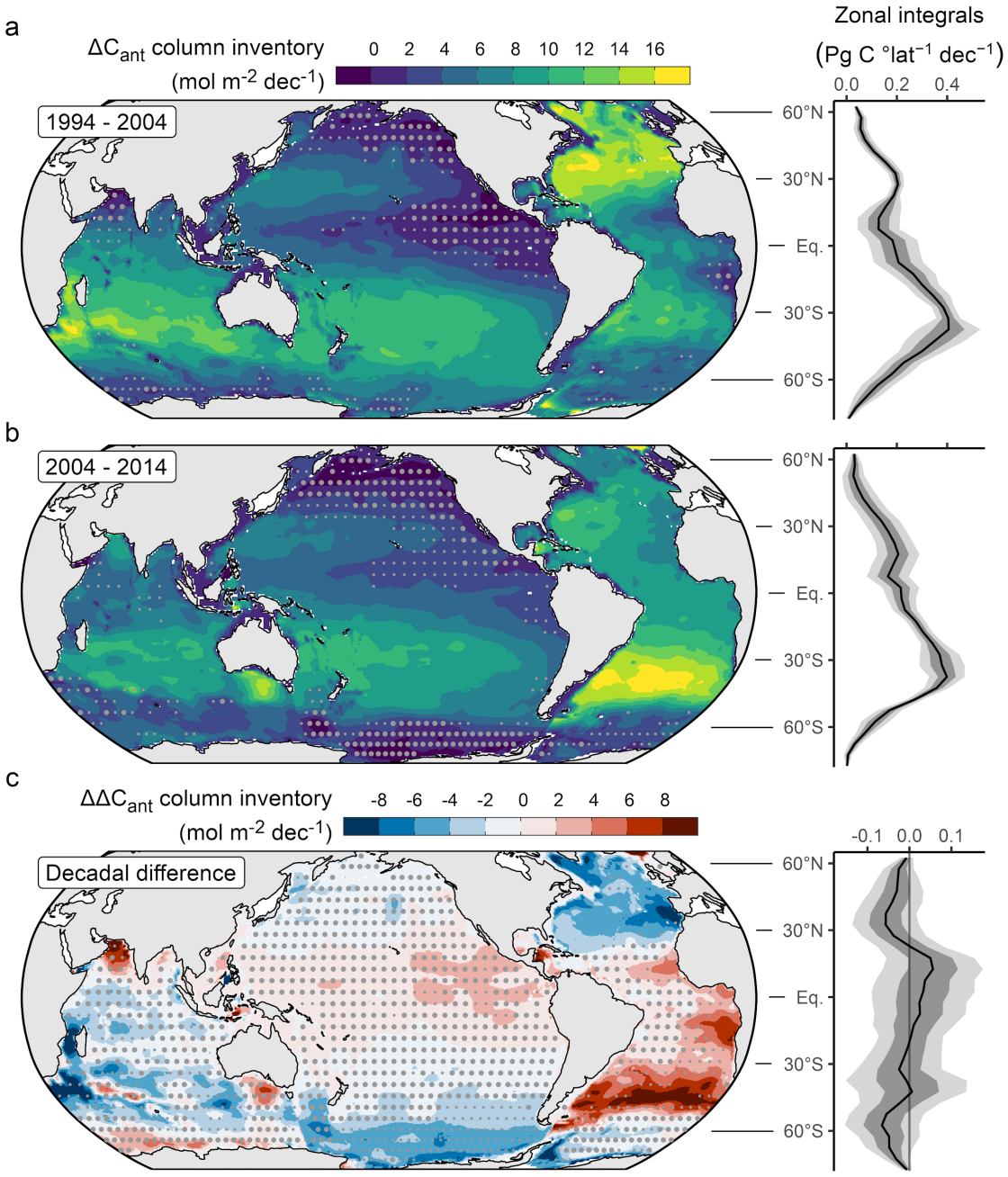

Fig. 2: Column inventory maps and zonal integrals of the storage change of anthropogenic carbon (ΔC_{ant}) integrated over the upper 3000m of the ocean for (a) 1994–2004 and (b) 2004–2014. Decadal differences in the storage changes ($\Delta\Delta C_{ant}$) are shown in (c). Plotted here are the results from the standard configuration. Stippling on the maps with small/large dots indicates regions in which the column inventories are lower than the respective 2σ-/1σ-uncertainty. Likewise, shading around the zonal integrals represents the 1σ- and 2σ-uncertainty ranges.

3.2 Vertical distribution

The high column inventories of ΔC_{ant} in the centres of the subtropical gyres seen in Figure 2a,b are due to a deeper penetration of ΔC_{ant} in these regions. This is illustrated by plotting

455 ΔC_{ant} along a global section (Fig. 3a,b) that connects the zonal mean sections of the Atlantic
456 and Pacific Ocean with a meridional mean section crossing the Indian Ocean sector of the
457 Southern Ocean. Within the subtropical gyres, ΔC_{ant} exceeding 5 µmol kg^{-1} dec^{-1} reaches at
458 least 300 m deeper than in the equatorial regions. This is primarily a consequence of the
459 passive tracer transport of C_{ant} along isopycnal surfaces (depicted in Fig. 3c), which brings
460 C_{ant} more rapidly into the ocean's interior in regions of downward sloping isopycnals (Bopp
461 et al., 2015; DeVries & Primeau, 2011). In the South Pacific, the ΔC_{ant} signal reaches deeper
462 into the water column compared to the North Pacific, which is a persistent pattern for both
463 decades and attributed to the formation of Subantarctic Mode and Antarctic Intermediate
464 Water (SAMW and AAIW). In contrast, in the Atlantic Ocean we identify a shift of the
465 deepest penetration of the ΔC_{ant} level of 5 µmol kg^{-1} dec^{-1} from the Northern to Southern
466 Hemisphere (Fig. 3c).

467 These changes in the downward extensions of ΔC_{ant} cause the decadal differences identified
468 in the column inventories of ΔC_{ant} in the Atlantic Ocean (Fig. 2c). The decrease of the mean
469 ΔC_{ant} column inventory in the North Atlantic is a consequence of the weaker C_{ant} storage
470 increase in the North Atlantic Deep Water (NADW), evident in the zonal mean section as
471 negative decadal differences (-2 to -5 µmol kg^{-1} dec^{-1}) at neutral densities >27.5 kg m^{-3} (Fig.
472 3c). In contrast, the decadal increase of the ΔC_{ant} column inventory in the South Atlantic can
473 be attributed to an intensified rate of C_{ant} storage in the Subantarctic Mode Waters (SAMW)
474 and Antarctic Intermediate Waters (AAIW). Here, positive ΔC_{ant} differences in the zonal
475 mean sections are well confined to the neutral density slabs ranging from 26.5 to 27.5 kg m^{-3}
476 (Fig. 3c). The decadal ΔC_{ant} differences in the NADW and the AAIW are larger than the
477 uncertainty of our reconstructions, while in most other water masses, the decadal differences
478 are not significant (stippling in Fig. 3c).

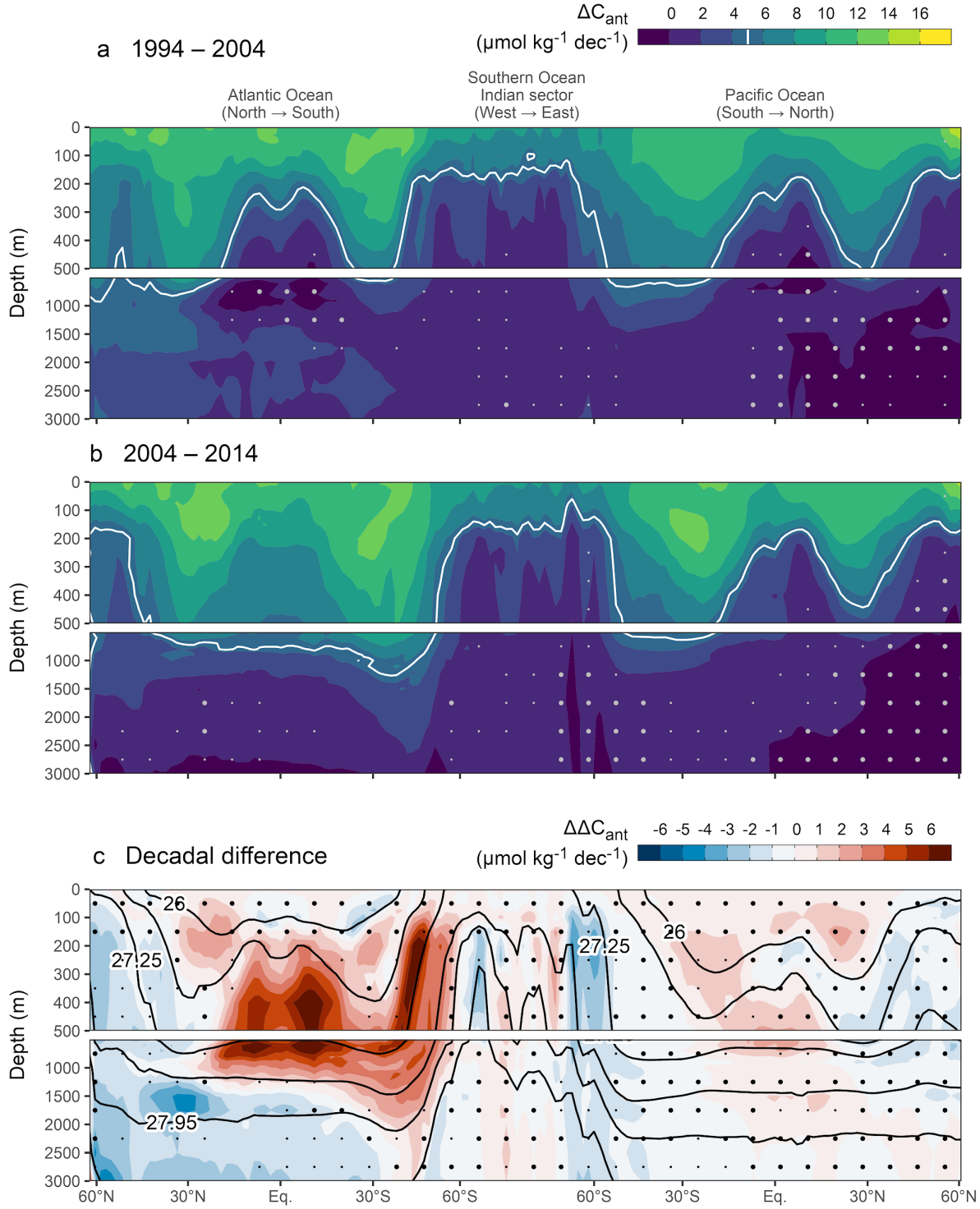

Fig. 3: Global sections of changes in the anthropogenic carbon content from north to south in the Atlantic Ocean, west to east in the Southern Ocean and south to north in the Pacific Ocean. The standard case reconstruction of ΔC_{ant} is shown for the decades (a) 1994–2004 and (b) 2004–2014. The white contour lines highlight the ΔC_{ant} level of 5 µmol kg^{-1} dec^{-1}. (c) Decadal differences between the storage changes ($\Delta\Delta C_{ant}$) shown in (a) and (c). Black contour lines in (c) indicate isoneutral density levels. The selected contours represent every second density slab used to cluster the data in the vertical dimension. Stippling with small or large dots indicates regions in which the ΔC_{ant} and $\Delta\Delta C_{ant}$

are lower than the 2σ- or 1σ-uncertainty, respectively. The North-South sections through the Atlantic and Pacific Ocean show zonal mean values across the entire basins, while the Southern Ocean sector is represented by a meridional mean section ranging from 55°S to 65°S that is compressed by a factor of 2.5 in distance. The location of the global section and areas for the computation of the zonal and meridional mean sections are displayed in Fig. S1.

Examining the vertical distribution of the reconstructed ΔC_{ant} in terms of area-weighted mean content profiles (Fig. 4a), we find that globally C_{ant} in the upper 50 m of the ocean increased on average by 10 – 11 µmol kg^{-1} dec^{-1} in both decades. As the storage change near the surface is determined based on an assumed equilibrium with the atmospheric CO_2, it shows latitudinal patterns that reflect gradients in the surface ocean buffer capacity (Fig. 3a,b). However, regional differences of the surface ΔC_{ant} averaged over hemispheric ocean basins are small (Fig. 4a). Furthermore, the almost identical surface ΔC_{ant} for both decades is due to a compensation of the higher atmospheric CO_2 growth rate and the reduced surface ocean buffer capacity in the second decade of our analysis. In contrast to the rather steady accumulation of C_{ant} in the surface ocean, the decadal differences in the mean ΔC_{ant} profiles tend to be more pronounced at depth in some regions. In the North Atlantic, ΔC_{ant} below 1000m is about 3 µmol kg^{-1} dec^{-1} lower during the second decade (Fig. 4a), while the mean ΔC_{ant} signal in the South Atlantic was significantly higher by about 3 µmol kg^{-1} dec^{-1} between 500 and 1500m during the second decade.

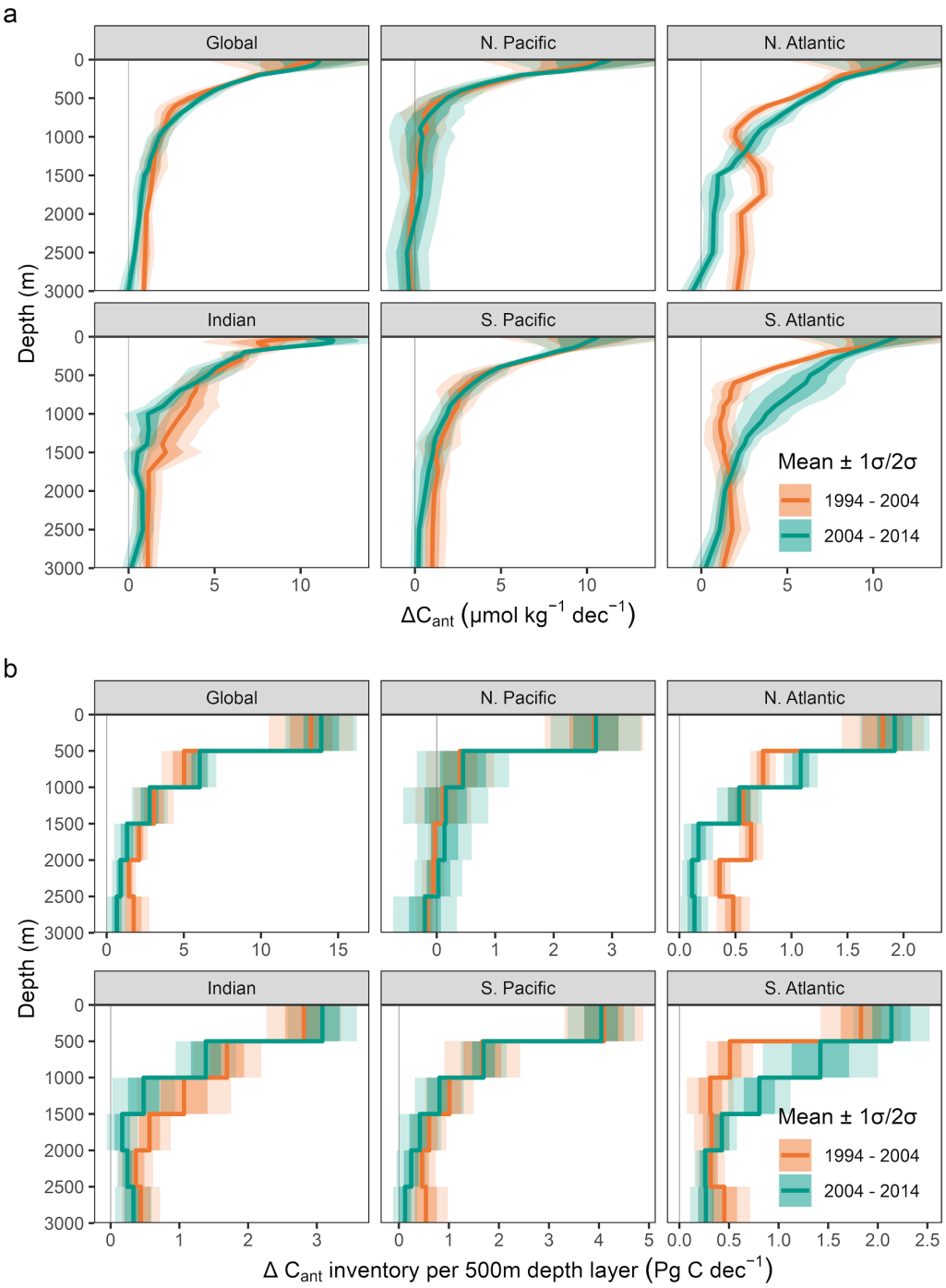

505 **Fig. 4**: Mean vertical distribution of the decadal changes in anthropogenic carbon (ΔC_{ant}) for the
506 global ocean and both hemispheres of the main ocean basins: (a) mean content profiles and (b) 500m-
507 depth layer inventories of ΔC_{ant}. Colours distinguish the decades 1994–2004 and 2004–2014. Thick
508 lines represent the standard case reconstruction of ΔC_{ant} and ribbons indicate the 1σ- and 2σ-
509 uncertainty ranges.

3.3 Regional and global inventories

Reflecting the rapid decrease of ΔC_{ant} with depth (Fig 4a), almost 50% of the global C_{ant} storage change occurs in the upper 500 m of the water column (Fig. 4b). Over the upper 1000 m, this share increases to around 75%, except in the North Pacific, where the entire inventory increase is fully confined to the top 1000 m. In all other ocean regions depicted in Figure 4b, a significant fraction of the C_{ant} storage change occurs below 1000 m (~25% on a global basis) as a result of the more rapid water mass transport and mixing between the surface and ocean interior in these regions. The decadal differences in the ΔC_{ant} inventories for 500 m depth layers reflect the profiles of the amount content and were found to be significant only in the three depth layers below 1500m of the North Atlantic, as well as between 500 and 1500 m in the South Atlantic (Fig. 4b).

Once integrated over the top 3000 m of entire ocean basins, (Fig. 5 and Table 1), the South Pacific stands out as the region with the highest increase of C_{ant} storage for both decades (1994–2004: 8.6 ± 1.2 Pg C dec^{-1} and 2004–2014: 7.4 ± 1.0 Pg C dec^{-1}), followed by the Indian Ocean (7.2 ± 0.9 and 5.7 ± 0.6 Pg C dec^{-1}). In contrast, the North Pacific accounts for the smallest contribution to the increase in the oceanic storage of C_{ant} in both decades (2.9 ± 0.8 and 3.2 ± 1.8 Pg C dec^{-1}). The decadal differences in the increases in C_{ant} storage are not significant at the 2σ-uncertainty level in any of these three regions. This is different for the North Atlantic (Fig. 5, Table 1), which represented the third largest sink region during the 1994–2004 decade (4.8 ± 0.2 Pg C dec^{-1}), but experienced a C_{ant} accumulation rate that was significantly reduced by 0.9 ± 0.4 Pg C dec^{-1} during the 2004–2014 period (3.9 ± 0.4 Pg C dec^{-1}). In contrast, the storage rate in the South Atlantic increased by 1.5 ± 0.8 Pg C dec^{-1} from the first (3.9 ± 0.5 PgC dec^{-1}) to the second decade (5.4 ± 0.6 Pg C dec^{-1}) of our analysis. As a consequence, the South Atlantic represents the third largest contributor to the global accumulation of C_{ant} from 2004 to 2014. The ranking of the ocean basins in terms of their contribution to the global ocean C_{ant} sink reflects primarily the differences in surface area of the basins.

The ranking of the regions changes markedly in terms of the area-normalised storage sensitivity β_{area} (Table 1 and Fig. S5), which is a measure of how much additional C_{ant} the ocean is storing within any given region in response to the increase in atmospheric CO_2 (see section 2.4). The North Atlantic has the highest regional storage sensitivity (25–40% larger than the global mean), and the North Pacific the lowest one (about 45–55% lower than the

global mean). This largely reflects the differences in intermediate, mode, and deep water formations between the different basins, and will be further discussed in section 4.1.

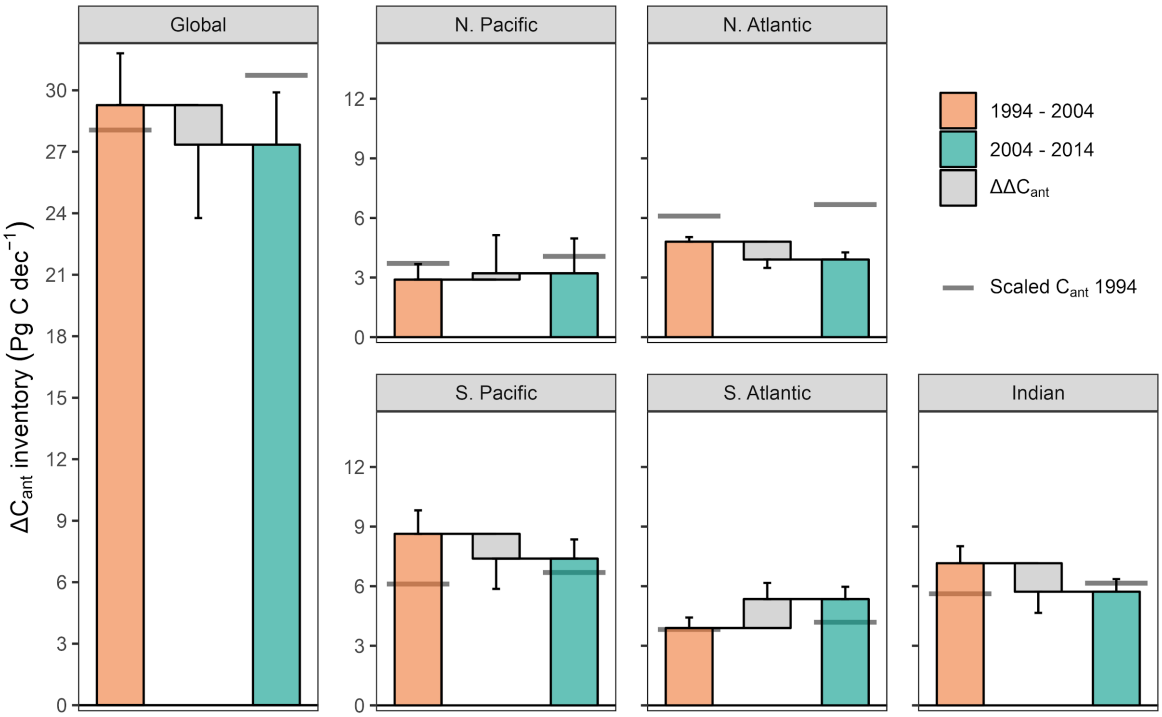

Fig. 5: Change in the storage of anthropogenic carbon (ΔC_{ant} inventory) integrated over the global ocean (left panel) and over the top 3000m for each hemisphere of the main ocean basins (right panels). Colored bars depict the inventory changes for the decades 1994–2004 and 2004–2014, and grey bars represent the decadal difference ($\Delta\Delta C_{ant}$ inventory). Error bars displayed in the direction of change represent the 1σ-uncertainty of each estimate. Horizontal lines indicate projected inventory changes based on the total C_{ant} storage in 1994 (Sabine et al., 2004) and assuming proportional growth with atmospheric CO_2 (see text for details).

When integrating ΔC_{ant} globally and scaling it for unmapped regions and deep water storage, we determine an ocean sink for anthropogenic CO_2 that amounts to 29.3 ± 2.5 and 27.3 ± 2.5 Pg C dec^{-1} for the 1994–2004 and the 2004–2014 decade, respectively (Fig. 5, Table 1). These inventory changes of C_{ant} are indistinguishable for both decades with a difference of -1.9 ± 3.6 Pg C dec^{-1}, indicating that the global ocean continued to act as a strong sink for anthropogenic CO_2 in the recent past. The global area-normalized storage sensitivity β_{area} decreased markedly and significantly, however, from 0.37 ± 0.03 mol m^{-2} ppm^{-1} for the decade 1994–2004 to 0.31 ± 0.03 mol m^{-2} ppm^{-1} during the second decade 2004–2014 (Table

559 1), suggesting a slowdown of the global ocean C_{ant} uptake relative to what one would expect
560 on the basis of the growth in atmospheric CO_2. For the 20-year period from 1994–2014, the
561 directly estimated global ΔC_{ant} inventory is identical to the sum of the estimates from the
562 individual decades (56.7 ± 3.5 Pg C dec^{-1}).

563 **Table 1**: Inventories of the change in anthropogenic carbon storage (ΔC_{ant} inventory) for the first
564 (1994–2004) and second (2004–2014) decade of our analysis, integrated separately across both
565 hemispheres of the main ocean basins and the global ocean. The inventory changes are further related
566 to the decadal growth rates in atmospheric CO_2 ($\Delta CO_{2,atm}$) to derive the sink sensitivity β in absolute
567 terms ($\beta = Inv(\Delta C_{ant}) / \Delta CO_{2,atm}$) and normalised to the surface area (A) of each ocean basin ($\beta_{area} = \beta /$
568 A in mol m^{-2} ppm^{-1}). †For consistency with the regional estimates, the global β_{area} estimate is based on
569 the directly mapped ΔC_{ant} inventory, whereas the global β estimate corresponds to the global ΔC_{ant}
570 inventory as given in this table, obtained by scaling the mapped inventory to global coverage. All
571 values refer to the standard cases of our ΔC_{ant} reconstruction and the corresponding 1σ-uncertainty
572 ranges. Decadal differences are tagged with ** or * when they exceed the combined 2σ- or 1σ-
573 uncertainty of both decades, respectively.

Parameter (unit)	**Region (Area in 10^6 km^2)**	**1994–2004**	**2004–2014**	**Decadal difference**
ΔC_{ant} inventory (Pg C dec^{-1})	**Global**	29 ± 2.5	27 ± 2.5	-1.9 ± 3.6
	N. Pacific	2.9 ± 0.8	3.2 ± 1.8	0.3 ± 1.9
	S. Pacific	8.6 ± 1.2	7.4 ± 1.0	-1.2 ± 1.5
	N. Atlantic	4.8 ± 0.2	3.9 ± 0.4	-0.9 ± 0.4 **
	S. Atlantic	3.9 ± 0.5	5.4 ± 0.6	1.5 ± 0.8 *
	Indian	7.2 ± 0.9	5.7 ± 0.6	-1.4 ± 1.1 *
$\Delta CO_{2,atm}$ (ppm dec^{-1})	**Global**	18.6	20.4	+1.8
β (Pg C ppm^{-1})	**Global†**	1.6 ± 0.1	1.3 ± 0.13	-0.23 ± 0.18 *
β_{area} (mol m^{-2} ppm^{-1})	**Global† (333)**	0.37 ± 0.03	0.31 ± 0.03	-0.05 ± 0.04 *
	N. Pacific (76)	0.17 ± 0.05	0.17 ± 0.09	0.002 ± 0.1
	S. Pacific (96)	0.40 ± 0.06	0.31 ± 0.04	-0.09 ± 0.07 *
	N. Atlantic (41)	0.53 ± 0.03	0.39 ± 0.04	-0.14 ± 0.04 **
	S. Atlantic (45)	0.39 ± 0.05	0.49 ± 0.06	0.1 ± 0.08 *
	Indian (73)	0.44 ± 0.05	0.32 ± 0.04	-0.12 ± 0.06 *

3.4 Uncertainty assessment

Nearly all identified main configuration choices of the eMRL(C*) method matter for the reconstruction of the decadal increases in C_{ant} and contribute to the uncertainties of the global inventory changes of about ±10% (Table 1, Figs. 6 and S9). The smallest uncertainty contributions stem from alternative definitions of C* and from uncertainties associated with the predictor climatologies used for mapping (Fig. 6). All other configuration choices matter more, although differently for the two decades, largely reflecting differences in the data distribution and data consistency.

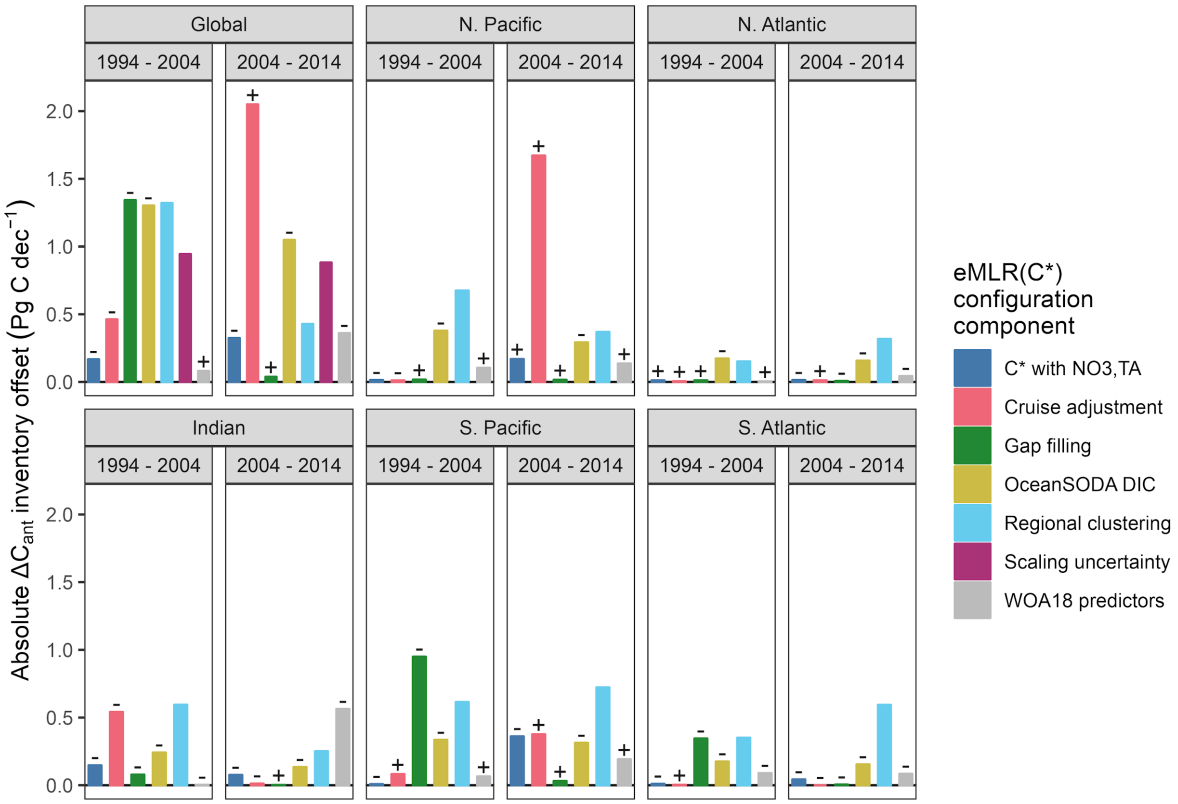

Fig. 6: Inventory uncertainty contributions at the 1σ-uncertainty level determined as offsets between our standard case reconstruction and six configuration choices of the eMLR(C*) method (colours) for each ocean region and both decades (panels). All offsets are shown as absolute values. Where applicable, +/- symbols on top of each bar indicate that higher/lower inventory changes were obtained when the configuration change was applied. The uncertainty contribution that accounts for our upscaling for unmapped water masses is shown for the global inventory.

The single largest contribution to the global inventory uncertainty comes from the way we

589 applied the adjustments to the DIC, TA and PO_4^{3-} measurements in order to ensure the highest
590 level of data consistency. If the adjustments were determined and applied separately for each
591 cruise instead of in a bulk manner as done in the standard configuration, the global ΔC_{ant}
592 inventories change by ~-0.5 Pg C dec^{-1} during the 2004-2014 period, and by ~+1.5 Pg C dec^{-1}
593 for the 2004-2014 period. Nearly all of the changes during the earlier decade originate at the
594 Indian Ocean, while those for the second period originate at the North Pacific (Figs. 6 and
595 S9), as expected given that these were the regions where we applied these adjustments.

596 The second most important uncertainty contribution comes from the regional clustering of the
597 observations with uncertainty contributions to the regional inventories ranging from 0.2 to 0.8
598 Pg C dec^{-1} (Figs. 6 and S9). However, for the global ΔC_{ant} inventories, the uncertainties
599 arising from the regional clustering partially cancel out, such that the global uncertainty
600 contribution is lower than the sum of the uncertainties in the individual basins (<1.5 Pg C
601 dec^{-1} for both decades, Fig. 6).

602 Among the other choices, the approach for the surface ΔC_{ant} reconstruction contributes about
603 1 Pg C dec^{-1} to the uncertainty of the global ΔC_{ant} inventory, determined by comparing our
604 estimate based on the assumption of surface ocean equilibrium of C_{ant} with a reconstruction
605 based on observation-based surface changes of DIC (Gregor & Gruber, 2021). Choices
606 associated with the gap filling also contribute about 1 Pg C dec^{-1} to the global uncertainty, but
607 this error source is limited largely to the first decade and the South Pacific (Fig. S9), where
608 we had to include a substantial number of cruises that took place in the 1990s and provided
609 only calculated TA data (Fig. 1). Finally, our scaling of the ΔC_{ant} inventories for unmapped
610 regions and the deep ocean introduces an additional uncertainty contribution of about 1 Pg C
611 dec^{-1}, however, confined to the global ΔC_{ant} inventories and of very similar magnitude for
612 both decades.

613 In addition to investigating the contribution of the configuration choices to the uncertainty of
614 our standard configuration, we also determined the sensitivity of our results to a set of
615 additional decisions we had to take for our reconstructions (see section S4.2). We did not add
616 these results to our formal uncertainty estimate since we consider our choices as well
617 justified, and the alternatives as clearly inferior choices. Among all these additional
618 decisions, we find that the biggest sensitivity of the results is associated with the data
619 adjustments in the North Pacific. Our reconstructions based on the unadjusted data reveal that

the ΔC_{ant} inventory in the North Pacific for the 2004 – 2014 period would be about 4 Pg C dec^{-1} higher than the standard case reconstruction (Fig. S11 and S12) that includes the adjustments. Hence, the global ΔC_{ant} inventory in the last decade would be higher than that obtained for the 1994 – 2004 period without North Pacific data adjustment. As a consequence, the growth of the C_{ant} inventory in the last decade would be roughly proportional to growth in atmospheric CO_2, such that we would interpret the storage sensitivity as unchanged over both decades and the industrial period. While multiple lines of evidence suggest that our data adjustments are justified and reflect inter-decadal measurement inconsistencies, the relevance of these adjustments for the interpretation of trends in the ocean carbon sink underpin the importance of long-term consistent ocean observations. Furthermore, we tested the sensitivity of our results to data coverage by reconstructing ΔC_{ant} with observations only from cruise sections that were reoccupied during both sampling periods. This reoccupation filter has generally a low impact on the reconstructed column inventories and basin inventories (Fig. S11 and S12), suggesting an overall sufficient data coverage. An exception to this are the ΔC_{ant} reconstructions in the Indian Ocean, which are more sensitive to the reoccupation filter (Fig. S11) due to the lack of data from the Arabian Sea during the central sampling period, i.e., the 2000s (Fig. 1B).

Our observation-based uncertainty and sensitivity findings are corroborated by our tests with synthetic data generated from an ocean hindcast model (supplement S5), following the approach developed by Clement and Gruber (2018). Comparing the biases of our reconstructed model inventories to the estimated uncertainty based on the configuration choices, we find that the bias of 7 (11) out of 12 reconstructed ΔC_{ant} inventories is within the 1σ- (2σ-) uncertainty range (Fig. S18), which meets the expectation of a 68% (95%) confidence interval. Our uncertainty ranges and confidence intervals are thus considered suitable criteria to evaluate the significance of our ΔC_{ant} reconstructions. Furthermore, the eMLR(C*) method proves capable of reconstructing the global ΔC_{ant} patterns (Fig. S13). The reconstruction biases of the ΔC_{ant} column inventories are below 2 mol m^{-2} dec^{-1} for 87% of the total ocean surface area, within 2 – 4 mol m^{-2} dec^{-1} for 13%, and only exceed the latter threshold for <0.5% of the surface area. In contrast, the true ΔC_{ant} column inventories in our model are larger than these thresholds of 2 and 4 mol m^{-2} dec^{-1} over more than 90 and 55% of the surface area of the ocean, respectively (Fig. S13a). In agreement with this assessment based on synthetic data, the observation-based ΔC_{ant} column inventories exceed the 1σ- and 2σ-uncertainty level over more than 90 and 75% of the total ocean surface area (Fig. 2a).

ΔC_{ant} column inventories that are lower than the local uncertainty are confined to regions with low ΔC_{ant} column inventories, primarily in the North Pacific (Fig. 2a). We conclude that the global distribution patterns of ΔC_{ant} are robustly reconstructed, which is in line with previous assessments of the method (Clement & Gruber, 2018) despite the shorter sampling periods applied in this study.

The tests with synthetic data subsampled from a GOBM are useful to demonstrate the skill of the eMLR(C*) method to reconstruct the inventory and spatial patterns of ΔC_{ant}. However, the tendency of the GOBMs to simulate a lower decadal variability of the ocean carbon sink compared to observation-based surface CO_2 flux products (Hauck et al., 2020) suggest that this testing approach may not be well suited to investigate the method's ability to detect decadal differences in the C_{ant} storage rates ($\Delta\Delta C_{ant}$). As a consequence of the model's low decadal variability, the spatial patterns in the column inventory biases show a strong correlation with the reconstructed $\Delta\Delta C_{ant}$ (Fig. S14 and S15). However, the observation-based $\Delta\Delta C_{ant}$ column inventories in the Atlantic Ocean (Fig. 2B) are higher than the $\Delta\Delta C_{ant}$ biases in the tests with synthetic data by about a factor of two (Fig. S15), suggesting that the observation-based $\Delta\Delta C_{ant}$ patterns carry, at least in part, a true signal.

3.5 Comparison with regional estimates

As a final component to assess the robustness of our estimates, we compare our ΔC_{ant} reconstructions to previous regional estimates that — same as our study — resolve changes for at least two periods and apply an MLR approach to ocean interior observations (see supplement S6 for details). Regional studies that fulfil these criteria are available for the North and South Atlantic (Gao et al., 2022; Wanninkhof et al., 2010; Woosley et al., 2016), as well as the North and South Pacific (Carter et al., 2019). We conclude from this comparison that the magnitude, patterns and trends in our ΔC_{ant} reconstructions agree with those determined in regional studies, and that differences can — where they exist — be attributed to differences in the chosen integration depth, differences in the definition of the target variable C*, and sometimes also to the uncertainty associated with the computation of a whole basin inventory from a single reoccupied transect (Gao et al., 2022; Woosley et al., 2016).

The most pronounced difference to a regional estimate exists in the South Pacific, where Carter et al. (2019) determined a change of the C_{ant} inventory of 5.4 ± 0.6 Pg C dec^{-1} from 1995 to 2005, whereas we determine a substantially higher inventory change of 8.6 ± 1.2 Pg C dec^{-1} for almost the same period (1994 – 2004). A main difference between these studies is the calculation of C* without (Carter et al., 2019) or with (this study) a TA contribution. Our sensitivity reconstruction of ΔC_{ant} in the South Pacific without considering the contribution of TA for the calculation of C* indeed reveals an inventory change that is about 3 Pg C dec^{-1} lower than our standard case reconstruction. Carter et al. (2019) relied on a synthetic data sensitivity test that included synthetic measurement uncertainties to conclude that the eMLR results are more robust for their implementation when the TA adjustment is omitted from the C* calculation. However, methodological differences between the methods used in that and our study limit the applicability of their sensitivity tests for our approach. We further contend that the additional attention paid to TA quality control results in better TA consistency between cruises than is assumed by Carter et al. (2019) and that the possibility of DIC changes driven by the calcium carbonate cycle (that are neither well represented in the synthetic data nor sufficiently correlated with nutrient and oxygen changes that they would be removed by following the eMLR approach) should not be neglected.

The second largest difference from a regional ΔC_{ant} inventory exists in the North Atlantic Ocean, where Wanninkhof et al. (2010) determined a C_{ant} storage rate of only 1.9 ± 0.4 Pg C dec^{-1} for the 1989–2003 period based on a single reoccupied cruise section. Their estimate is drastically lower than ours for the 1994–2004 decade (4.8 ± 0.2 Pg C dec^{-1}). Our tests of the eMLR(C*) method reveal that the uncertainty of our estimates can only explain a minor part of this offset. We conclude that the offset is primarily due to differences in the integration depth, structural uncertainties in the regional estimate (Wanninkhof et al., 2010) and extrapolation errors from a single reoccupied cruise section to a whole basin inventory. In fact, Woosley et al. (2016) found that the whole basin inventories of the North Atlantic differ by ~30% when comparing estimates obtained from a single section to those obtained from three sections.

In general, the individual differences between our regional ΔC_{ant} inventories and those obtained in the previous regional studies are within the uncertainty range of our global inventory. Therefore, we do not assume that offsets at the regional scale challenge the robustness and interpretation of our global inventories.

4 Discussion

4.1 Decadal trends or *the ocean at a time of change*

Our ocean-interior observation-based reconstruction of the changes in the global oceanic storage of anthropogenic carbon reveal for the two consecutive decades since 1994 indistinguishable accumulation rates, i.e., 29.3 ± 2.5 Pg C dec^{-1} and 27.3 ± 2.5 Pg C dec^{-1} for 1994–2004 and 2004–2014, respectively (Fig. 5, Table 1). Putting this continued accumulation of anthropogenic carbon into the context of the total oceanic C_{ant} storage in 1994 (118 ± 19 Pg C), we confirm the expected linear correlation with the increase in atmospheric CO_2 (Fig. 7, see also Gruber et al., 2023). But for a more detailed and quantitative discussion of the recent decadal trends in the ocean carbon sink, it is informative to look at potential changes in the slope of this relationship, i.e., changes in the global sensitivity β and the associated area-normalised sensitivity β_{area} (see section 3.3). For the global sensitivity β, we compute values of 1.6 ± 0.1 Pg C ppm^{-1} and 1.3 ± 0.1 Pg C ppm^{-1} for the two decades, respectively (Table 1, Fig. 7). Their average confirms the long-term mean value of 1.4 ± 0.1 Pg C ppm^{-1} diagnosed by Gruber et al. (2023), but the significant decrease of about 15 ± 11% between the two decades indicates a weakening of the ocean sink for C_{ant}. The reason that this difference in β is significant, while the 7 ± 12% reduction (-1.9 ± 3.6 Pg C dec^{-1}) in the global ΔC_{ant} inventory is not, is due to the ~10% higher growth rate in atmospheric CO_2 from 2004 to 2014 compared to that during the previous decade (Table 1).

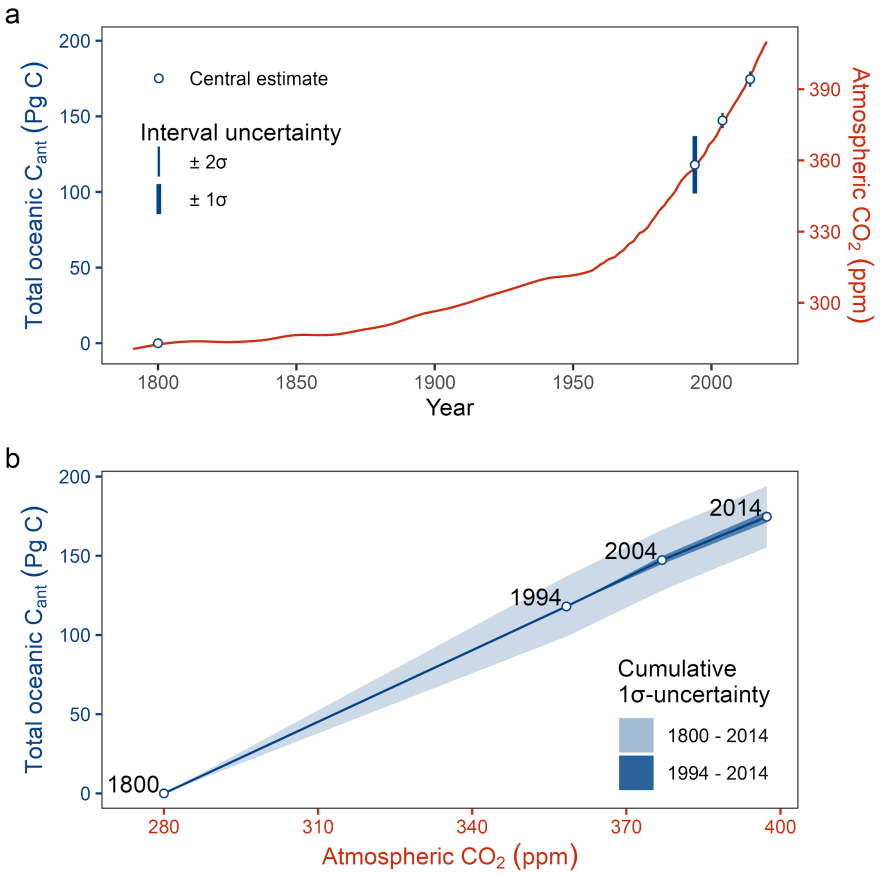

733 **Fig. 7**: Total C_{ant} accumulation in the ocean interior from 1800–2014, shown in blue as a function of
734 (a) time and (b) atmospheric CO_2. Total C_{ant} was estimated by adding our global C_{ant} inventory
735 changes (Table 1) to the total C_{ant} inventory in 1994 (118 ± 19 Pg C) according to Sabine et al. (2004).
736 The red line in (a) shows the time history of atmospheric CO_2. The cumulative uncertainty in (b) for
737 the 1994–2014 period (dark blue ribbon) assumes zero uncertainty in 1994.

738 As the ocean acidifies in response to taking up CO_2, a decrease of the ocean sink efficiency is
739 expected due to the decrease of the ocean buffer capacity (Jiang et al., 2019). Over the past
740 40 years, seawater that followed the same pCO_2 increase as the atmosphere would have
741 experienced a ~6% reduction of the DIC increase per change in pCO_2 roughly every ten
742 years. This estimate is based on fundamental marine CO_2-system considerations and reflects
743 an increase in the Revelle factor (Sarmiento & Gruber, 2006). The 6% decadal weakening of
744 the ability of the surface ocean carbonate chemistry to buffer the increase in pCO_2 can
745 explain about half of the observed decrease in the sink sensitivity β. The other half is most
746 likely attributable to changes in the ocean's circulation and upper ocean stratification (Sallée
747 et al., 2021) that appears to have led to a less efficient downward transport of C_{ant}, which we
748 discuss further in the following.

Roughly half of the decrease of the global ocean carbon sink stems from the reduced decadal storage changes in the North Atlantic (-0.9 ± 0.4 Pg C dec^{-1}). Here, we find a significant weakening of the area-normalised sink sensitivity β_{area} (-0.14 ± 0.04 mol m^{-2} ppm^{-1}) when comparing the first (1994–2004) to the second decade (2004–2014) of our analysis (Table 1, Figs. S4,S5). Furthermore, our β_{area} estimates for both decades are well below that obtained for the 1800–1994 period (Sabine et al., 2004), indicating a progressive weakening of the sink efficiency in the North Atlantic. The most plausible explanation for this progressive weakening is a tendency of the Atlantic Meridional Overturning Circulation (AMOC) to weaken since the 1980s (L. C. Jackson et al., 2019; Laura C. Jackson et al., 2022; Latif et al., 2022). Attributing the decadal ΔC_{ant} differences to changes in AMOC strength is supported by the localization of the negative $\Delta\Delta C_{ant}$ signal in the North Atlantic Deep Water (Fig. 3c). This view is also in line with two previous sets of regional studies: (i) (F. F. Pérez et al., 2010; Fiz F. Pérez et al., 2013) found that the C_{ant} storage rates in the North Atlantic subpolar gyre during the phase of a low North Atlantic Oscillation (NAO) from 1997–2006 were ∼48% lower than those during the first half of the 1990s, when a high NAO phase was dominant, although the mechanistic processes linking the NAO, subpolar convection strength, gyre circulation and the AMOC are not yet fully understood. (ii) Raimondi et al. (2021) reconstructed C_{ant} column inventories in the Central Labrador Sea based on CFC-12 observations and identified a period of near zero C_{ant} increases between 2003 and 2012.

However, an important caveat regarding our finding of a progressively weakening North Atlantic C_{ant} sink is the fact that the available ocean interior observations in the North Atlantic stem mostly from the first half of our last sampling period, the 2010s. However, after 2013 the NAO switched to a strong positive phase (Holliday et al., 2020) and in line with this, the C_{ant} column inventories in the Central Labrador Sea rapidly increased (Raimondi et al., 2021). Likewise, a deep convection event in the Irminger Sea in winter 2014/15 injected anthropogenic carbon into the ocean interior and almost tripled the storage rates compared to those determined from previous hydrographic sections (F. Fröb et al., 2016). It is thus possible that our reconstructions do not capture a very recent reinvigoration of the North Atlantic C_{ant} sink, due to the temporal distribution of the available observations.

The decadal difference of the South Atlantic C_{ant} sink is significant at the 1σ-uncertainty level (+1.5 ± 0.8 Pg C dec^{-1}) and slightly exceeds the increase expected from the growth in

780 atmospheric CO_2 alone, expressed in an increase of the sink sensitivity (+0.1 ± 0.08 mol m^{-2}
781 ppm^{-1}). In contrast to the North Atlantic, the decadal change in the South Atlantic is not of
782 progressive nature when putting it into context of the total C_{ant} storage until 1994 (Fig. 5), i.e.,
783 only the second decade reveals a tendency towards an elevated storage sensitivity. Due to the
784 strong spatial coherence between the positive $\Delta\Delta C_{ant}$ signal and the Subantarctic Mode and
785 Antarctic Intermediate Waters (Fig. 3c), we attribute the decadal differences found in the
786 South Atlantic to increased ventilation rates of these water masses (DeVries et al., 2017;
787 Panassa et al., 2018; Patara et al., 2021; Shi et al., 2021).

788 Although the decadal inventory changes in the Indian Ocean and South Pacific are much less
789 robust than those in the Atlantic, they represent in sum a contribution of about 2.6 ± 1.9 Pg C
790 dec^{-1} to the decline of the global inventory. As the negative $\Delta\Delta C_{ant}$ signals in these regions are
791 associated primarily with Antarctic Bottom Water and Lower Circumpolar Deep Waters (Fig.
792 S7), the decadal differences in the C_{ant} storage changes are likely a consequence of circulation
793 changes as well, albeit determined with lower uncertainty than in other regions.

794 An additional, and globally perhaps more uniform, contribution to the decrease may stem
795 from the observed increase in upper ocean stratification (Sallée et al., 2021). Sallée et al.
796 found that the density contrast across the base of the mixed layer had increased by about 9%
797 per decade between 1970 and 2018. Although their estimate pertains only to the summer,
798 such an increase in stratification is bound to decrease the transport of C_{ant} from the surface to
799 depth, i.e., the most important bottleneck for the uptake of C_{ant} from the atmosphere.

800 We conclude that in addition to the decrease of the ocean buffer capacity, ocean circulation
801 changes and the increase in stratification are likely to play an important role in driving the
802 decrease in the sink sensitivity, i.e., the strength of the oceanic sink for anthropogenic carbon
803 per unit change in atmospheric CO_2.

804 **4.2 Comparison with observation-based surface flux estimates: Implications for changes**
805 **in the natural carbon storage**

806 In the following, we compare our estimates of the global oceanic sink of anthropogenic
807 carbon to an ensemble of observation-based surface CO_2 flux products assembled by the
808 Global Carbon Budget (Friedlingstein et al., 2022). During the 1994–2004 decade, the ocean

interior accumulation of anthropogenic carbon (29.3 ± 2.5 Pg C dec^{-1}) exceeds the time-integrated net air-sea flux of CO_2 of 21.4 ± 2.8 Pg C dec^{-1} (Fig. 8 and Table 2). For this comparison, we followed GCB procedures and adjusted the observation-based air-sea fluxes for a preindustrial steady-state outgassing of riverine CO_2 of 6.1 Pg C dec^{-1} (Jacobson et al., 2007; Resplandy et al., 2018) without considering the uncertainty contribution from this adjustment. We further excluded the air-sea flux estimates provided by Watson et al. (2020) when calculating the ensemble mean and standard deviation of the flux products (see separate analysis below). Analogous to Gruber et al. (2019), the difference between the ocean interior estimates and the surface fluxes of 7.9 ± 3.8 Pg C dec^{-1} can plausibly be interpreted as a loss of natural carbon from the ocean to the atmosphere (Table 2). Such natural carbon fluxes are captured by the surface flux products, but are not included in the eMLR(C*) based estimates of the accumulation of C_{ant} in the ocean's interior (Clement & Gruber, 2018). The 1σ-uncertainty of this residual term is almost half as large as the signal itself, suggesting that while the determined flux is significant, its magnitude is not well constrained. However, postulating a loss of natural carbon for the first decade of our analysis is qualitatively in line with previous studies, which concluded that the stagnation of the ocean carbon sink during the 1990s is due to an anomalously strong outgassing of natural carbon primarily in the Southern Ocean (Landschützer et al., 2015; Le Quéré et al., 2007; Lovenduski et al., 2008). It should be noted that our approach to determine the natural carbon flux as a residual term between the net surface flux and the storage change of anthropogenic carbon is only possible at global scale, because storage changes at regional scales can also occur due to ocean interior transport of anthropogenic carbon.

For the 2004–2014 decade, there is no significant difference between the cumulative surface CO_2 fluxes (26.5 ± 1.3 Pg C dec^{-1}) and our ocean interior ΔC_{ant} inventory (27.3 ± 2.5 Pg C dec^{-1}), suggesting only a minor global net flux of natural CO_2 across the air-sea interface (0.9 ± 2.9 Pg C dec^{-1}). The fact that during the second decade the gain of anthropogenic and the loss of natural carbon weakened simultaneously can plausibly be explained by a weakened ventilation of the ocean interior, induced by changes in circulation and/or stratification (Sallée et al., 2021), which results in lower upward transport rates of natural carbon to the surface and, vice versa, reduced downward transport of C_{ant} into the ocean interior. This coupling was already hypothesised in previous studies that identified a synchronised reduction of both carbon flux components during periods of a weak upper-ocean overturning circulation (DeVries et al., 2017; Lovenduski et al., 2008). Specifically, DeVries et al. (2017)

suggested a more vigorous global overturning in the 1990s that drove an increased outgassing of natural CO_2 and uptake of anthropogenic CO_2, whereas a weaker overturning in the 2000s was found to have the opposite effect. Although the periods of our and their study do not fully overlap, the tendencies toward a weaker anthropogenic carbon uptake agree.

The synchronisation of the uptake of anthropogenic and the outgassing of natural carbon was also observed at a regional scale in the Irminger Sea, where Fröb et al. (2018) detected a sharp increase of the C_{ant} inventory from 2012 to 2015, accompanied by a decline in the natural carbon inventory. This was attributed to a deep convection event during 2015 (Fröb et al., 2016), and underlines that variability at regional scale can superimpose upon the postulated global trend towards a declining anthropogenic carbon uptake.

Our determination of the natural carbon flux as a residual component relies sensitively on the underlying estimates of the net surface CO_2 flux. Watson et al. (2020) recently suggested that the current pCO_2-based flux estimates are all biassed low due to their lack of consideration of near-surface temperature gradients. When taking these temperature gradients into consideration, they estimated an ocean carbon sink that is up to 50% larger than the unadjusted estimate. If we used their adjusted flux estimate instead of the ensemble mean of the other flux products as a basis for our calculation of the natural carbon flux (Fig. 8), we would determine a release of natural carbon of 5.5 ± 3.8 Pg C dec^{-1} for the period 1994–2004 and an uptake of -4.0 ± 2.9 Pg C dec^{-1} for the period 2004–2014. Hence, we would find a weaker loss of natural carbon during the first decade and an uptake of natural carbon rather than a near-zero flux during the second decade. The integral of the natural carbon flux over the two decades would be near zero rather than a net loss. Thus, if we used the temperature adjusted CO_2 flux estimate of Watson et al. (2020), the absolute values of our globally-integrated natural carbon flux estimates would change, but this substitution would not change the conclusion that these fluxes are subject to substantial decadal variability. We note that a recent re-evaluation of the temperature adjustments by Dong et al. (2022) concluded that the effects are likely smaller than suggested by Watson et al. (2022). With the nature and magnitude of these temperature adjustments not yet settled by the community, we stay with the ensemble of unadjusted CO_2 fluxes, but emphasise that the absolute magnitude of the natural CO_2 fluxes inferred from our work may be subject to future revisions. Another need for later revision might arise in the future if recent indications that some ensemble members of the surface flux products overestimate the true decadal variability proved to be correct

(Gloege et al., 2021). A final need for revision might arise if our suggested adjustments of the North Pacific data turn out to be erroneous. This would cause no change in the C_{nat} outgassing estimated for the first decade, but it would make the C_{nat} flux larger (more outgassing) during the second decade. In conclusion, there is strong indication that the natural CO_2 flux has been responding sensitively to recent climate change and variability, but the current estimates underpinning the estimation of this component come with too many caveats to provide a hard constraint.

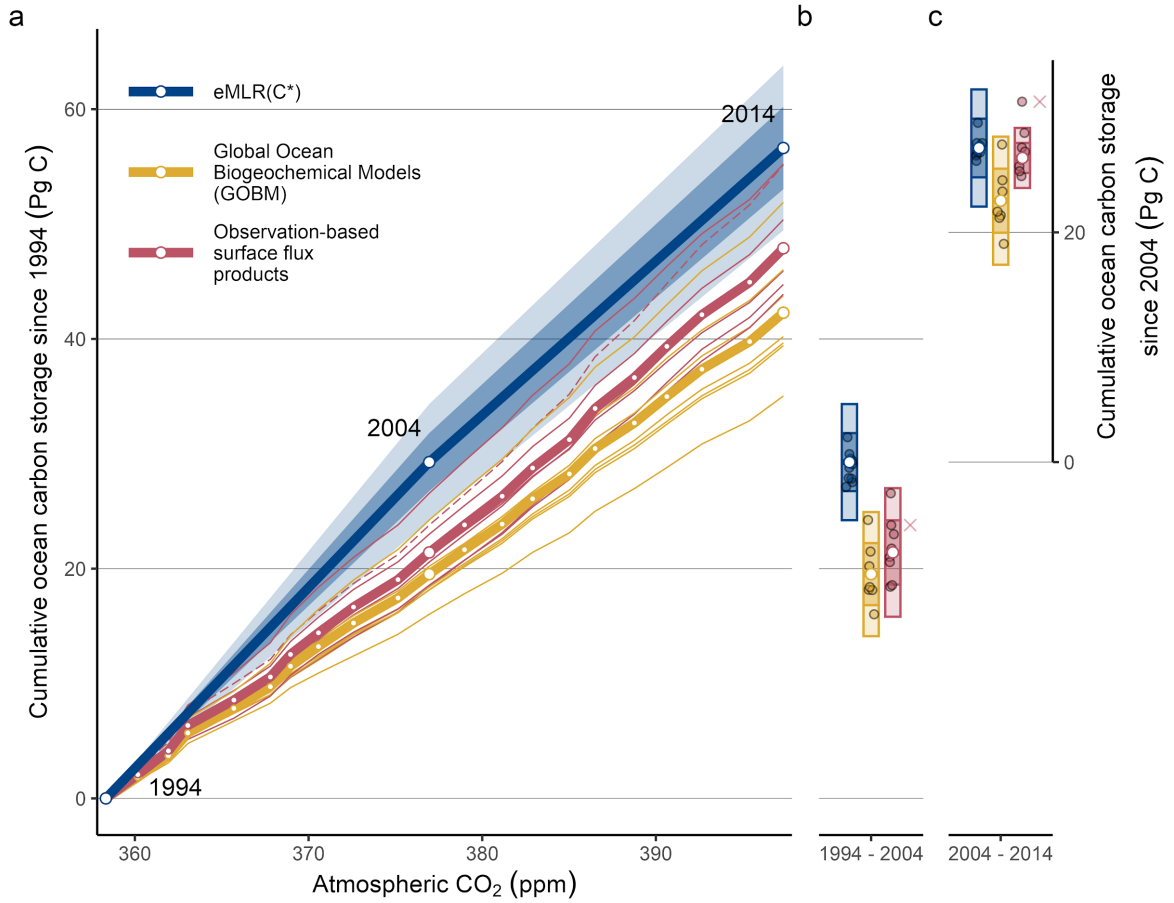

Fig. 8: Ocean carbon storage from 1994 to 2014 according to the eMLR(C*) estimates from this study (blue), in comparison to the cumulative fluxes from surface pCO_2 observation-based air-sea CO_2 flux products (red) and Global Ocean Biogeochemical Models (yellow) from the Global Carbon Budget. The ocean carbon storage is displayed in (a) as a function of atmospheric pCO_2 and in (b and c) as separate temporal integrals across the two decades of our study. All cumulative estimates for the 2004–2014 period in (c) use the eMLR(C*) estimate for 2004 as the zero point. White points represent the ensemble mean for the GCB estimates and the standard case for the eMLR(C*) estimates. Bars in (b and c) indicate 1σ- and 2σ-uncertainty ranges. The dashed line in (a) and crosses in (b) and (c) represent a CO_2 flux product that is not included in the ensemble and accounts for near-surface temperature gradients (Watson et al., 2020). Note: The eMLR(C*) estimates represent storage changes of anthropogenic carbon only, while the GCB estimates include fluxes of natural and

anthropogenic CO_2 (see detailed discussion in the main text).

4.3 Implications for the Global Carbon Budget and climate change

During the first decade of our study (1994–2004), the flux estimates of the GOBMs (19.5 ± 2.7 Pg C dec^{-1}) and the observation-based flux products (21.4 ± 2.8 Pg C dec^{-1}) are significantly lower than the eMLR(C*)-based estimate (29.3 ± 2.5 Pg C dec^{-1}). In the previous section, we proposed climate-driven outgassing of natural CO_2 from the ocean as a plausible explanation for the discrepancy to the surface flux products. The same argument would apply to the GOBMs, as their flux estimate includes the natural CO_2 flux component. For the 2004–2014 period, the difference between the cumulative observation-based surface fluxes and the ocean interior storage change of C_{ant} disappears, suggesting only a minor global net outgassing of natural CO_2. However, the GOBMs (22.8 ± 2.7 Pg C dec^{-1}, Fig. 8) still diagnose a 17 % weaker ocean carbon sink during the second decade compared to our ocean interior estimates. The most likely explanation for this discrepancy lies in a combination of three challenges that the majority of the current generation of GOBMs are facing: (i) the surface to deep ocean transport of C_{ant} is rather sluggish, as these ocean models tends to underestimate the ventilation rates of the ocean interior, which was illustrated in structurally similar Earth System Models (Fu et al., 2022; Terhaar et al., 2022), (ii) the GOBMs reveal a generally lower decadal variability of the CO_2 fluxes compared to observation-based estimates (Gloege et al., 2021; Hauck et al., 2020), and (iii) the non steady-state fluxes of natural CO_2 (i.e., the fluxes that are caused by climate variability) appear to be low in the GOBMs. For example in the CESM-ETHZ model used in this study, the cumulative flux of natural CO_2 over the 1994–2004 period amounts only to a net uptake of 0.1 Pg C dec^{-1}, and ranges in terms of annual fluxes from an outgassing of 0.2 Pg C yr^{-1} and an uptake of 0.4 Pg C yr^{-1}, which is substantially lower than the observation-based estimate determined in this study.

Considering these three challenges of the GOBMs, the decadal offsets compared to both observation-based estimates (surface and interior) could be explained as follows: During the first decade, the GOBMs simulate a low anthropogenic CO_2 uptake and a low outgassing of natural CO_2. The compensation of these two biases leads to an apparent agreement with the surface-flux and ocean interior estimates. For the second decade, the anthropogenic CO_2

uptake in the GOBMs remains low, but this bias is no longer compensated for by the bias in the outgassing of natural CO_2. While this interpretation of the decadal differences between the three groups of estimates is internally consistent, we emphasise that most of the evaluated offsets are of similar magnitude as their uncertainties. A more bottom-up assessment requires the comparison of the different carbon flux components for the ensemble of GOBMs reported in the GCB, an effort that is currently underway in the framework of phase 2 of the REgional Carbon Cycle Assessment and Processes (RECCAP2) project (Poulter et al., 2022).

To put our ocean carbon sink estimates over the last two decades further into the context of the global carbon cycle, we compare them with the evolution of anthropogenic carbon emissions, as well as with the land and the atmospheric carbon sink extracted from the Global Carbon Budget 2021 (Friedlingstein et al., 2022) for the same periods (Table 2). From this comparison we derive the airborne, ocean-borne and land-borne fraction of the total emissions (Table 2). The ocean-borne fraction of anthropogenic carbon is computed by dividing, for the respective periods, the oceanic sink with the total anthropogenic emissions following the procedures in the GCB (Friedlingstein et al., 2022). In analogy, we report the airborne and land-borne fractions by relating the increase in the atmospheric CO_2 inventory or the land carbon sink to the anthropogenic emissions of CO_2. Note that the global sensitivity β, is directly related to these fractions, since it is the ratio between the ocean- and airborne fraction. For the total anthropogenic emissions we consider the emissions due to the combustion of fossil fuels (including the cement carbonation sink) and land use change.

An important aspect for the contextualisation of our ocean sink estimates is the increase of the total emissions by about 25% from the first to the second decade of our analysis. In contrast, the growth of the atmospheric sink for CO_2 was only about 10% higher during the second decade, which is reflected in a decrease of the airborne fraction from 48 ± 4 % to 44 ± 4 %. Because the emissions grew more rapidly than the atmospheric CO_2, the ocean-borne fraction of C_{ant} (Table 2) decreases even more pronouncedly than the global ocean's uptake sensitivity β (Table 1), namely from 36 ± 4 % to 27 ± 4 % for the 1994–2004 and 2004–2014 decade, respectively, which corresponds to a reduction of the uptake fraction of -9 ± 6% (or ~25% in relative terms). In contrast, the land sink evolved very consistently with the total emissions over the two decades, such that the land-borne fraction remained at a stable level (31 ± 6 % and 30 ± 6 %). Due to the identified oceanic outgassing of natural carbon during the first but not the second decade of our analysis, the net ocean sink for anthropogenic and

natural carbon increases in a remarkably stable manner with the total emissions. Accordingly, the ocean-borne fraction of the total emissions in terms of the net oceanic CO_2 uptake remained unchanged at a level of 26 ± 4 % and 26 ± 3 %. According to our assessment, the sum of all three sink estimates exceeds the total emissions by about 5% during the 1994–2004 period, whereas the sources and sinks of CO_2 during the 2004–2014 period match almost perfectly.

Table 2: Main sources and sinks of CO_2 for the periods 1994–2004 and 2004–2014 in Pg C dec^{-1}. Estimates of emissions, and the atmospheric, land and net ocean sink are based on the Global Carbon Budget 2021 (Friedlingstein et al., 2022). The net ocean sink estimates represent the cumulative surface fluxes based on surface-pCO_2 observations, adjusted for the outgassing of riverine carbon. The oceanic sink estimates of C_{ant} are from this study, and the oceanic outgassing of natural carbon was determined as the residual between the C_{ant} and the net ocean sink. The uncertainties of the oceanic sink estimates follow the approach of this study, and for all other estimates apply the relative uncertainties for the 2000s according to Table 6 in the GCB. Numbers in parentheses indicate the airborne, land-borne, and ocean-borne fractions in % of the total emissions, with propagated uncertainties from the total emissions and the sink terms.

CO_2 sources sinks	**1994–2004 (Pg C dec^{-1})**	**2004–2014 (Pg C dec^{-1})**
Total emissions	81.8 ± 7.3	100.3 ± 8.9
Fossil emissions	68.3 ± 3.5	88.2 ± 4.6
Land-use change emissions	13.5 ± 7.9	12 ± 7
Atmospheric sink	39.3 ± 0.2	44 ± 0.2
(Airborne fraction)	(48 ± 4 %)	(44 ± 4 %)
Land sink	25 ± 4.8	29.8 ± 5.7
(Land-borne fraction)	(31 ± 6 %)	(30 ± 6 %)
Ocean sink of C_{ant}	29.3 ± 2.5	27.3 ± 2.5
(Ocean-borne fraction of C_{ant})	(36 ± 4 %)	(27 ± 4 %)
Inferred outgassing of natural carbon	7.9 ± 3.8	0.9 ± 2.9
Net ocean sink	21.4 ± 2.8	26.5 ± 1.3
(Net ocean-borne fraction)	(26 ± 4 %)	(26 ± 3 %)

Although we do not identify a change in the net ocean-borne fraction of the total emissions between 1994 and 2014, it is not for granted that the ocean carbon sink will remain constant for the decades to come (Ridge & McKinley, 2021). DeVries et al. (2017) hypothesised that a

trend towards a more stratified ocean is likely to strengthen the CO_2 sink in the near future by trapping natural CO_2 in the deep ocean, but further concluded that this process may ultimately limit the net oceanic carbon sink, when the reduced uptake of anthropogenic CO_2 that continues to accumulate in the atmosphere outweighs the reduced outgassing of natural carbon. Our findings demonstrate that these compensating processes are in progress and we deem it of utmost importance to continue the monitoring of the ocean interior accumulation of carbon to keep track of them.

4.4 Caveats and Recommendations

Building on the quantitative uncertainty assessment of our ΔC_{ant} reconstructions (section 3.4, supplement S4 and S5), we highlight in the following some caveats of our study and provide recommendations on how to overcome them in future studies.

While all sampling periods assigned for this study are relatively well covered with observations, the large changes we reconstruct in the North Atlantic between the first and second period need to be viewed with caution since the number of data records that provide all required variables for the eMLR(C*) analysis is very limited after ~2015. During this period, a reinvigoration of the anthropogenic carbon accumulation has been reported in regional studies (Friederike Fröb et al., 2018; Raimondi et al., 2021), albeit only for small subregions of the whole North Atlantic. The inclusion of North Atlantic observations collected since 2015 into an eMLR(C*)-based ΔC_{ant} reconstruction will contribute to further improve our understanding of the basin-wide C_{ant} storage changes in this highly dynamic region.

We further expect substantially new and improved insights from the completion of another cycle of the repeat hydrography programme over the 2020s. In contrast to our two decadal ΔC_{ant} reconstructions, which both build on the same data for the central sampling period (2000s) and are thus not fully independent, reconstructing ocean interior trends with yet another decade of observations would resolve this issue. Furthermore, future investigations based on more recent data will profit from the improved data quality, in particular when becoming independent from the observations of the 1990s, which tend to be less consistent than the more recent measurements (Lauvset et al., 2021).

The continued tracking of the oceanic C_{ant} storage, e.g., by providing a global ΔC_{ant} reconstruction for the 2014–2024 period, would also shed light on the very recent divergence of GOBMs and surface-flux products which increased to more than 1 Pg C yr^{-1} in 2020 (Friedlingstein et al., 2022; Hauck et al., 2020). A burning question in this regard is whether the high uptake determined by the surface flux products around 2020 can be confirmed by ocean interior estimates. Scaling our C_{ant} accumulation estimates from the 2004–2014 period to the 2010s according to the atmospheric CO_2 increase, we would indeed project an uptake of ~32 Pg C dec^{-1}, which is very similar to the mean observation-based net surface flux over the same period.

Another recommendation emerges from the high sensitivity of our results to the adjustments we applied to a subset of the observations provided through GLODAPv2.2021. This pronounced sensitivity highlights the importance of data quality and consistency for the ocean interior observing system. Continued efforts to maintain and improve the quality of seawater biogeochemical measurements, such as through the continued use of reference materials and undertaking inter-laboratory comparisons (Bockmon & Dickson, 2015), are indispensable. Furthermore, the timely submission, compilation, and harmonisation of data through GLODAP appears crucial. The release of version 3 of GLODAP including a complete revision of the data adjustments is anticipated in 2024. Based on our findings, we suggest a critical revision of the observation from the Pacific with a particular focus on the TA measurements.

Tightly linked to the observational data consistency is the accuracy of deep ocean ΔC_{ant} reconstructions. Small biases in ΔC_{ant} can indeed exert a strong impact on the basin inventory changes due to the large volume of the deep ocean. Below 1000 m, the mean ΔC_{ant} reconstructed in this study is lower than 5 µmol kg^{-1} dec^{-1} across all ocean basins (Fig. 4a). Despite the low ΔC_{ant} rates compared to surface waters, the ocean below 1000 m represents a potentially significant contribution to the global C_{ant} inventory as it accounts for roughly 75% of the total ocean volume. On a global average the content and inventory changes between 1000 and 3000 m carry a significant positive signal and contribute about 25% to the total inventory integrated over the top 3000 m. To derive our global inventories, we have chosen to account for the storage change below 3000 m (~30% of the total ocean volume) by scaling the inventory with +2% according to the total C_{ant} accumulation at depth in 1994 (Sabine et al., 2004). This approach is consistent with previous studies (Gruber et al., 2019) and

represents a compromise between neglecting deep water storage changes and potentially introducing biases from integrating small and highly uncertain ΔC_{ant} below 3000m. It is important to note that the general decadal trends reported in this study for the regional inventories are maintained when integrating the reconstructed ΔC_{ant} across the full water column, i.e., without the deep ocean scaling (data not shown). Nevertheless, we deem it important that future observation-based studies explicitly include also the accumulation of anthropogenic carbon in the deep ocean below 3000 m water depth, taking advantage, for example, of measurements of transient tracers, such as SF_6 and CFCs.

Finally, our study revealed that fluxes of natural carbon are key to understanding the oceanic response to a changing climate. The comparison of our estimates of the ocean interior accumulation of anthropogenic carbon with the net surface fluxes of CO_2 allowed us to distinguish a decade with presumably strong net outgassing of natural carbon (1994–2004) from a decade with low net fluxes of natural carbon (2004–2014). However, our quantification of the natural carbon flux as a residual quantity between two entirely independent estimates remains prone to uncertainties that are in the same order of magnitude as the flux itself (B. I. McNeil & Matear, 2013). This uncertainty is partly due to remaining uncertainties in the estimates of the surface flux products, some of which might tend to overestimate decadal variability and could be prone to systematic biases such as a missing consideration of near-surface temperature gradients. Furthermore, our testing of the eMLR(C*) method based on synthetic data from a single GOBM with low decadal variability in the anthropogenic carbon storage (see section 3.4) and low changes in the natural carbon pool (see section 4.3) impedes a comprehensive assessment of the method's ability to quantify decadal variability and separate changes in the inventories of natural and anthropogenic carbon. Tests of the method over a larger ensemble of GOBMs, with artificially perturbed data, or time-variant predictor variables may allow further investigation of this aspect. As natural carbon fluxes are expected to vary substantially at sub-decadal time scales, a reoccupation of selected repeat hydrography sections with increased frequency or the extension of the BGC Argo programme to global coverage could provide an important observational basis for future studies of ocean interior carbon dynamics. Furthermore, progress in the development of statistical methods to separate storage changes of natural and anthropogenic carbon based on a consistent interpretation of ocean interior observations alone could provide new valuable insight. The application of neural networks to reconstruct ocean interior dynamics of DIC are a meaningful first step in this direction (Broullón et al.,

2019, 2020; Keppler et al., 2020, 2023), albeit being based on even fewer data than surface pCO_2 products

5 Conclusion and Outlook

This study provides the first global reconstruction of the decadal evolution of the ocean interior storage changes of anthropogenic carbon covering the decades 1994 to 2004 and 2004 to 2014. We provide uncertainty estimates for all reported estimates, including regional inventories and spatial distributions of ΔC_{ant}, and decompose the uncertainties into contributions from various configuration choices associated with the eMLR(C*) method.

We find that the oceanic sink for anthropogenic carbon remained strong during both decades (29 ± 3 PgC dec^{-1} and 27 ± 3 PgC dec^{-1}, respectively). But the sink strength relative to the growth in atmospheric CO_2 (sensitivity β) and the uptake fraction of anthropogenic emissions weakened from the first to the second decade by about 15 and 25%, respectively. We attribute these changes to a decrease of the ocean buffer capacity and a reduction in the surface ocean to deep transport, induced by changes in ocean circulation (most apparent in the Atlantic) and an increase in upper ocean stratification. In contrast to our findings for the accumulation of C_{ant}, observation-based estimates of the surface fluxes of CO_2 indicate that the net ocean sink for anthropogenic and natural carbon increased proportionally with the anthropogenic emissions. This implies that the net ocean uptake fraction remained stable throughout both decades. We attribute the difference between the anthropogenic and the net carbon sink to substantial fluxes of natural carbon that vary between decades, but remain hard to quantify.

Our results can serve as new reference points for the annual ocean sink estimates published in the Global Carbon Budget and provide guidance to further develop and assess global ocean biogeochemical models, which most likely underestimate the anthropogenic carbon sink. Furthermore, our reconstructions of the continuing accumulation of C_{ant} can be used to infer acidification trends in the ocean interior at global scale.

Future studies of the ocean interior storage of C_{ant} may allow us to address questions arising from our analysis, including the drivers for the very recent increase in the net uptake flux as determined based on surface pCO_2-observations and the question whether compensating

processes of the ocean carbon cycle remain effective, such as the regional shift of the anthropogenic carbon storage from the North to the South Atlantic and the apparent coupling between the fluxes of natural and anthropogenic carbon. Mandatory requirements to address these topics are (i) the continued and extended collection of biogeochemical ocean interior observations, i.e. the completion of a fourth cycle of the repeat hydrography programme and the expansion of the biogeochemical Argo programme to global coverage, (ii) the continued compilation of the observations into a harmonised and quality-controlled data product, and (iii) the continued improvement and further development of statistical methods, for example to separate the storage changes of anthropogenic and natural carbon.

Acknowledgments

The authors thank all colleagues that supported and contributed to the collection and harmonisation of high-quality ocean interior observations made available through GLODAP. We are grateful for the formal reviewer comments provided by Andrew Watson and two anonymous reviewers, as well as the informal comments provided on a preprint of this manuscript by Judith Hauck and Jens Terhaar. JDM and NG acknowledge support from the European Union's Horizon 2020 research and innovation programme under grant agreements no. 821003 (project 4C) and no. 821001 (SO-CHIC). FFP was supported by the BOCATS2 (PID2019-104279GB-C21) project funded by MCIN/AEI/10.13039/501100011033 and contributed to WATER:iOS CSIC PTI. AO and SKL were supported by the project N-ICOS-2 (Research Council of Norway grant no 296012). SKL also acknowledges internal funding support from NORCE. MI was supported by JPMEERF21S20810. RW, RAF, and BC were supported by the Office of Ocean and Atmospheric Research (OAR) of NOAA, including the Global Observation and Monitoring Program (GOMO), FundRef 100018302. BC and RAF contributions are PMEL contribution 5454 and CICOES contribution 2022-1244. TT acknowledges support by EU Horizon 2020 through the EuroSea action (grant agreement 862626).

Conflict of Interest

The authors declare no conflicts of interest relevant to this study.

Open Research

The anthropogenic carbon estimates reconstructed in this study are available through the Research Collection of ETH Zurich under the Creative Commons licence Attribution 4.0 International (CC BY 4.0) via the digital object identifier:
https://doi.org/10.3929/ethz-b-000590910
Upon acceptance of this manuscript for publication, a copy of this data set will be made available through NCEI's Ocean Carbon and Acidification Data System (OCADS), which is accessible under:
https://www.ncei.noaa.gov/products/ocean-carbon-acidification-data-system

All observational data sets underlying our analysis are publicly available.

The merged master file of GLODAPv2.2021 as well as the mapped climatology based on GLODAPv2 were accessed through:
www.glodap.info
The World Ocean Atlas 2018 climatology data and basin masks were accessed through:
https://www.ncei.noaa.gov/products/world-ocean-atlas
The global gridded data set of the surface ocean carbonate system (OceanSODA-ETHZ) is available under:
https://doi.org/10.25921/m5wx-ja34

For review purposes, the code used to preprocess the data sets, apply the eMLR(C*) method and analyse the generated output is available in these three github repositories:
https://github.com/jens-daniel-mueller/emlr_obs_preprocessing
https://github.com/jens-daniel-mueller/emlr_obs_v_XXX
https://github.com/jens-daniel-mueller/emlr_obs_analysis
The final version of the code will be made available through Zenodo via a digital object identifier upon acceptance of this manuscript for publication

References

Bittig, H. C., Steinhoff, T., Claustre, H., Fiedler, B., Williams, N. L., Sauzède, R., et al. (2018). An Alternative to Static Climatologies: Robust Estimation of Open Ocean CO2 Variables and Nutrient Concentrations From T, S, and O2 Data Using Bayesian Neural Networks. *Frontiers in Marine Science*, *5*. https://doi.org/10.3389/fmars.2018.00328

Bockmon, E. E., & Dickson, A. G. (2015). An inter-laboratory comparison assessing the quality of seawater carbon dioxide measurements. *Marine Chemistry*, *171*, 36–43. https://doi.org/10.1016/j.marchem.2015.02.002

Bopp, L., Lévy, M., Resplandy, L., & Sallée, J. B. (2015). Pathways of anthropogenic carbon subduction in the global ocean. *Geophysical Research Letters*, *42*(15), 6416–6423. https://doi.org/10.1002/2015GL065073

Broullón, D., Pérez, F. F., Velo, A., Hoppema, M., Olsen, A., Takahashi, T., et al. (2019). A global monthly climatology of total alkalinity: a neural network approach. *Earth System Science Data*, *11*(3), 1109–1127. https://doi.org/10.5194/essd-11-1109-2019

Broullón, D., Pérez, F. F., Velo, A., Hoppema, M., Olsen, A., Takahashi, T., et al. (2020). A global monthly climatology of oceanic total dissolved inorganic carbon: a neural network approach. *Earth System Science Data*, *12*(3), 1725–1743. https://doi.org/10.5194/essd-12-1725-2020

Carter, B. R., Feely, R. A., Wanninkhof, R., Kouketsu, S., Sonnerup, R. E., Pardo, P. C., et al. (2019). Pacific Anthropogenic Carbon Between 1991 and 2017. *Global Biogeochemical Cycles*, 2018GB006154. https://doi.org/10.1029/2018GB006154

Cheng, L., Foster, G., Hausfather, Z., Trenberth, K. E., & Abraham, J. (2022). Improved Quantification of the Rate of Ocean Warming. *Journal of Climate*, *35*(14), 4827–4840. https://doi.org/10.1175/JCLI-D-21-0895.1

1174 Clement, D., & Gruber, N. (2018). The eMLR(C*) Method to Determine Decadal Changes in
1175 the Global Ocean Storage of Anthropogenic CO $_2$. *Global Biogeochemical Cycles*,
1176 *32*(4), 654–679. https://doi.org/10.1002/2017GB005819
1177 Crisp, D., Dolman, H., Tanhua, T., McKinley, G. A., Hauck, J., Bastos, A., et al. (2022).
1178 How Well Do We Understand the Land-Ocean-Atmosphere Carbon Cycle? *Reviews*
1179 *of Geophysics*, *60*(2), e2021RG000736. https://doi.org/10.1029/2021RG000736
1180 DeVries, T. (2014). The oceanic anthropogenic CO2 sink: Storage, air-sea fluxes, and
1181 transports over the industrial era. *Global Biogeochemical Cycles*, *28*(7), 631–647.
1182 https://doi.org/10.1002/2013GB004739
1183 DeVries, T., & Primeau, F. (2011). Dynamically and Observationally Constrained Estimates
1184 of Water-Mass Distributions and Ages in the Global Ocean. *Journal of Physical*
1185 *Oceanography*, *41*(12), 2381–2401. https://doi.org/10.1175/JPO-D-10-05011.1
1186 DeVries, T., Holzer, M., & Primeau, F. (2017). Recent increase in oceanic carbon uptake
1187 driven by weaker upper-ocean overturning. *Nature*, *542*(7640), 215–218.
1188 https://doi.org/10.1038/nature21068
1189 Dickson, A. G, & Riley, J. P. (1979). The estimation of acid dissociation constants in
1190 seawater media from potentionmetric titrations with strong base. I. The ionic product
1191 of water — Kw. *Marine Chemistry*, *7*(2), 89–99. https://doi.org/10.1016/0304-
1192 4203(79)90001-X
1193 Dickson, Andrew G. (1990). Standard potential of the reaction: AgCl(s) + 12H2(g) = Ag(s) +
1194 HCl(aq), and and the standard acidity constant of the ion HSO4− in synthetic sea
1195 water from 273.15 to 318.15 K. *The Journal of Chemical Thermodynamics*, *22*(2),
1196 113–127. https://doi.org/10.1016/0021-9614(90)90074-Z
1197 Doney, S. C., Lima, I., Feely, R. A., Glover, D. M., Lindsay, K., Mahowald, N., et al. (2009).
1198 Mechanisms governing interannual variability in upper-ocean inorganic carbon

1199 system and air–sea CO2 fluxes: Physical climate and atmospheric dust. *Deep Sea*
1200 *Research Part II: Topical Studies in Oceanography*, *56*(8), 640–655.
1201 https://doi.org/10.1016/j.dsr2.2008.12.006
1202 Dong, Y., Bakker, D. C. E., Bell, T. G., Huang, B., Landschützer, P., Liss, P. S., & Yang, M.
1203 (2022). Update on the Temperature Corrections of Global Air-Sea CO2 Flux
1204 Estimates. *Global Biogeochemical Cycles*, *36*(9), e2022GB007360.
1205 https://doi.org/10.1029/2022GB007360
1206 Fay, A. R., Gregor, L., Landschützer, P., McKinley, G. A., Gruber, N., Gehlen, M., et al.
1207 (2021). SeaFlux: harmonization of air–sea CO_2 fluxes from surface pCO_2 data
1208 products using a standardized approach. *Earth System Science Data*, *13*(10), 4693–
1209 4710. https://doi.org/10.5194/essd-13-4693-2021
1210 Friedlingstein, P., Jones, M. W., O'Sullivan, M., Andrew, R. M., Bakker, D. C. E., Hauck, J.,
1211 et al. (2022). Global Carbon Budget 2021. *Earth System Science Data*, *14*(4), 1917–
1212 2005. https://doi.org/10.5194/essd-14-1917-2022
1213 Fröb, F., Olsen, A., Våge, K., Moore, G. W. K., Yashayaev, I., Jeansson, E., & Rajasakaren,
1214 B. (2016). Irminger Sea deep convection injects oxygen and anthropogenic carbon to
1215 the ocean interior. *Nature Communications*, *7*(1), 13244.
1216 https://doi.org/10.1038/ncomms13244
1217 Fröb, Friederike, Olsen, A., Pérez, F. F., García-Ibáñez, M. I., Jeansson, E., Omar, A., &
1218 Lauvset, S. K. (2018). Inorganic carbon and water masses in the Irminger Sea since
1219 1991. *Biogeosciences*, *15*(1), 51–72. https://doi.org/10.5194/bg-15-51-2018
1220 Fu, W., Moore, J. K., Primeau, F., Collier, N., Ogunro, O. O., Hoffman, F. M., & Randerson,
1221 J. T. (2022). Evaluation of Ocean Biogeochemistry and Carbon Cycling in CMIP
1222 Earth System Models With the International Ocean Model Benchmarking (IOMB)
1223 Software System. *Journal of Geophysical Research: Oceans*, *127*(10),

e2022JC018965. https://doi.org/10.1029/2022JC018965

Gammon, R. H., Cline, J., & Wisegarver, D. (1982). Chlorofluoromethanes in the northeast Pacific Ocean: Measured vertical distributions and application as transient tracers of upper ocean mixing. *Journal of Geophysical Research: Oceans*, *87*(C12), 9441–9454. https://doi.org/10.1029/JC087iC12p09441

Gao, H., Cai, W.-J., Jin, M., Dong, C., & Timmerman, A. H. V. (2022). Ocean Ventilation Controls the Contrasting Anthropogenic CO2 Uptake Rates Between the Western and Eastern South Atlantic Ocean Basins. *Global Biogeochemical Cycles*, *36*(6), e2021GB007265. https://doi.org/10.1029/2021GB007265

Gattuso, J.-P., Epitalon, J.-M., Lavigne, H., & Orr, J. (2021). seacarb: Seawater Carbonate Chemistry. Retrieved from https://CRAN.R-project.org/package=seacarb

Gloege, L., McKinley, G. A., Landschützer, P., Fay, A. R., Frölicher, T. L., Fyfe, J. C., et al. (2021). Quantifying Errors in Observationally Based Estimates of Ocean Carbon Sink Variability. *Global Biogeochemical Cycles*, *35*(4), e2020GB006788. https://doi.org/10.1029/2020GB006788

Graham, F. S., & McDougall, T. J. (2013). Quantifying the Nonconservative Production of Conservative Temperature, Potential Temperature, and Entropy. *Journal of Physical Oceanography*, *43*(5), 838–862. https://doi.org/10.1175/JPO-D-11-0188.1

Gregor, L., & Gruber, N. (2021). OceanSODA-ETHZ: a global gridded data set of the surface ocean carbonate system for seasonal to decadal studies of ocean acidification. *Earth System Science Data*, *13*(2), 777–808. https://doi.org/10.5194/essd-13-777-2021

Gruber, N., & Sarmiento, J. L. (2002). Large-scale biogeochemical/physical interactions in elemental cycles. In A. R. Robinson, J. J. McCarthy, & B. J. Rothschild (Eds.), *THE SEA: Biological-Physical Interactions in the Oceans* (Vol. 12, pp. 337–399). New York, NY: John Wiley and Sons.

1249 Gruber, N., Sarmiento, J. L., & Stocker, T. F. (1996). An improved method for detecting
1250 anthropogenic CO2 in the oceans. *Global Biogeochemical Cycles*, *10*(4), 809–837.
1251 https://doi.org/10.1029/96GB01608
1252 Gruber, N., Clement, D., Carter, B. R., Feely, R. A., van Heuven, S., Hoppema, M., et al.
1253 (2019). The oceanic sink for anthropogenic CO2 from 1994 to 2007. *Science*,
1254 *363*(6432), 1193–1199. https://doi.org/10.1126/science.aau5153
1255 Gruber, N., Bakker, D. C. E., DeVries, T., Gregor, L., Hauck, J., Landschützer, P., et al.
1256 (2023). Trends and variability in the ocean carbon sink. *Nature Reviews Earth &*
1257 *Environment*, 1–16. https://doi.org/10.1038/s43017-022-00381-x
1258 Hauck, J., Zeising, M., Le Quéré, C., Gruber, N., Bakker, D. C. E., Bopp, L., et al. (2020).
1259 Consistency and Challenges in the Ocean Carbon Sink Estimate for the Global
1260 Carbon Budget. *Frontiers in Marine Science*, *7*.
1261 https://doi.org/10.3389/fmars.2020.571720
1262 Holliday, N. P., Bersch, M., Berx, B., Chafik, L., Cunningham, S., Florindo-López, C., et al.
1263 (2020). Ocean circulation causes the largest freshening event for 120 years in eastern
1264 subpolar North Atlantic. *Nature Communications*, *11*(1), 585.
1265 https://doi.org/10.1038/s41467-020-14474-y
1266 IPCC. (2019). *IPCC Special Report on the Ocean and Cryosphere in a Changing Climate*
1267 *[H.-O. Pörtner, D.C. Roberts, V. Masson-Delmotte, P. Zhai, M. Tignor, E.*
1268 *Poloczanska, K. Mintenbeck, A. Alegría, M. Nicolai, A. Okem, J. Petzold, B. Rama,*
1269 *N.M. Weyer (eds.)]*. Cambridge University Press.
1270 https://doi.org/10.1017/9781009157964
1271 Jackson, L. C., Dubois, C., Forget, G., Haines, K., Harrison, M., Iovino, D., et al. (2019). The
1272 Mean State and Variability of the North Atlantic Circulation: A Perspective From
1273 Ocean Reanalyses. *Journal of Geophysical Research: Oceans*, *124*(12), 9141–9170.

https://doi.org/10.1029/2019JC015210

Jackson, Laura C., Biastoch, A., Buckley, M. W., Desbruyères, D. G., Frajka-Williams, E., Moat, B., & Robson, J. (2022). The evolution of the North Atlantic Meridional Overturning Circulation since 1980. *Nature Reviews Earth & Environment*, 1–14. https://doi.org/10.1038/s43017-022-00263-2

Jacobson, A. R., Fletcher, S. E. M., Gruber, N., Sarmiento, J. L., & Gloor, M. (2007). A joint atmosphere-ocean inversion for surface fluxes of carbon dioxide: 2. Regional results. *Global Biogeochemical Cycles*, *21*(1). https://doi.org/10.1029/2006GB002703

Jiang, L.-Q., Carter, B. R., Feely, R. A., Lauvset, S. K., & Olsen, A. (2019). Surface ocean pH and buffer capacity: past, present and future. *Scientific Reports*, *9*(1), 18624. https://doi.org/10.1038/s41598-019-55039-4

Keeling, C. D. (1979). The Suess effect: 13Carbon-14Carbon interrelations. *Environment International*, *2*(4), 229–300. https://doi.org/10.1016/0160-4120(79)90005-9

Keppler, L., Landschützer, P., Gruber, N., Lauvset, S. K., & Stemmler, I. (2020). Seasonal Carbon Dynamics in the Near-Global Ocean. *Global Biogeochemical Cycles*, *34*(12), e2020GB006571. https://doi.org/10.1029/2020GB006571

Keppler, L., Landschützer, P., Lauvset, S. k., & Gruber, N. (2023). Recent trends and variability in the oceanic storage of dissolved inorganic carbon. *Global Biogeochemical Cycles*, *n/a*(n/a). https://doi.org/10.1029/2022GB007677

Key, R. M., Kozyr, A., Sabine, C. L., Lee, K., Wanninkhof, R., Bullister, J. L., et al. (2004). A global ocean carbon climatology: Results from Global Data Analysis Project (GLODAP). *Global Biogeochemical Cycles*, *18*(4). https://doi.org/10.1029/2004GB002247

Khatiwala, S., Primeau, F., & Hall, T. (2009). Reconstruction of the history of anthropogenic CO 2 concentrations in the ocean. *Nature*, *462*(7271), 346–349.

https://doi.org/10.1038/nature08526

Khatiwala, S., Tanhua, T., Mikaloff Fletcher, S., Gerber, M., Doney, S. C., Graven, H. D., et al. (2013). Global ocean storage of anthropogenic carbon. *Biogeosciences*, *10*(4), 2169–2191. https://doi.org/10.5194/bg-10-2169-2013

Lan, X., Tans, P., & Thoning, K. W. (2022). Trends in globally-averaged CO2 determined from NOAA Global Monitoring Laboratory measurements. Version 2022-11 NOAA/GML (gml.noaa.gov/ccgg/trends/).

Landschützer, P., Gruber, N., Haumann, F. A., Rödenbeck, C., Bakker, D. C. E., van Heuven, S., et al. (2015). The reinvigoration of the Southern Ocean carbon sink. *Science*, *349*(6253), 1221–1224. https://doi.org/10.1126/science.aab2620

Landschützer, P., Gruber, N., & Bakker, D. C. E. (2016). Decadal variations and trends of the global ocean carbon sink. *Global Biogeochemical Cycles*, *30*(10), 1396–1417. https://doi.org/10.1002/2015GB005359

Latif, M., Sun, J., Visbeck, M., & Hadi Bordbar, M. (2022). Natural variability has dominated Atlantic Meridional Overturning Circulation since 1900. *Nature Climate Change*, 1–6. https://doi.org/10.1038/s41558-022-01342-4

Lauvset, S. K., Key, R. M., Olsen, A., van Heuven, S., Velo, A., Lin, X., et al. (2016). A new global interior ocean mapped climatology: the 1◦ × 1◦ GLODAP version 2, 16.

Lauvset, S. K., Lange, N., Tanhua, T., Bittig, H. C., Olsen, A., Kozyr, A., et al. (2021). An updated version of the global interior ocean biogeochemical data product, GLODAPv2.2021. *Earth System Science Data*, *13*(12), 5565–5589. https://doi.org/10.5194/essd-13-5565-2021

Lauvset, S. K., Lange, N., Tanhua, T., Bittig, H. C., Olsen, A., Kozyr, A., et al. (2022). GLODAPv2.2022: the latest version of the global interior ocean biogeochemical data product. *Earth System Science Data*, *14*(12), 5543–5572. https://doi.org/10.5194/essd-

14-5543-2022

Le Quéré, C., Rödenbeck, C., Buitenhuis, E. T., Conway, T. J., Langenfelds, R., Gomez, A., et al. (2007). Saturation of the Southern Ocean CO2 Sink Due to Recent Climate Change. *Science*, *316*(5832), 1735–1738. https://doi.org/10.1126/science.1136188

Li, G., Cheng, L., Zhu, J., Trenberth, K. E., Mann, M. E., & Abraham, J. P. (2020). Increasing ocean stratification over the past half-century. *Nature Climate Change*, 1–8. https://doi.org/10.1038/s41558-020-00918-2

Locarnini, R., Mishonov, A., Baranova, O., Boyer, T., Zweng, M., Garcia, H., et al. (2019). *World Ocean Atlas 2018, Volume 1: Temperature*.

Lovenduski, N. S., Gruber, N., & Doney, S. C. (2008). Toward a mechanistic understanding of the decadal trends in the Southern Ocean carbon sink. *Global Biogeochemical Cycles*, *22*(3). https://doi.org/10.1029/2007GB003139

Lueker, T. J., Dickson, A. G., & Keeling, C. D. (2000). Ocean pCO2 calculated from dissolved inorganic carbon, alkalinity, and equations for K1 and K2: validation based on laboratory measurements of CO2 in gas and seawater at equilibrium. *Marine Chemistry*, *70*(1), 105–119. https://doi.org/10.1016/S0304-4203(00)00022-0

McNeil, B. I., & Matear, R. J. (2013). The non-steady state oceanic CO_2 signal: its importance, magnitude and a novel way to detect it. *Biogeosciences*, *10*(4), 2219–2228. https://doi.org/10.5194/bg-10-2219-2013

McNeil, Ben I., Matear, R. J., Key, R. M., Bullister, J. L., & Sarmiento, J. L. (2003). Anthropogenic CO2 Uptake by the Ocean Based on the Global Chlorofluorocarbon Data Set. *Science*, *299*(5604), 235–239. https://doi.org/10.1126/science.1077429

Olsen, A., Omar, A. M., Jeansson, E., Anderson, L. G., & Bellerby, R. G. J. (2010). Nordic seas transit time distributions and anthropogenic CO2. *Journal of Geophysical Research: Oceans*, *115*(C5). https://doi.org/10.1029/2009JC005488

1349 Olsen, A., Key, R. M., van Heuven, S., Lauvset, S. K., Velo, A., Lin, X., et al. (2016). The
1350 Global Ocean Data Analysis Project version 2 (GLODAPv2) – an internallyconsistent
1351 data product for the world ocean. *Earth System Science Data*, *8*(2), 297–323.
1352 https://doi.org/10.5194/essd-8-297-2016
1353 Palmiéri, J., Orr, J. C., Dutay, J.-C., Béranger, K., Schneider, A., Beuvier, J., & Somot, S.
1354 (2015). Simulated anthropogenic CO_2 storage and acidification of the Mediterranean
1355 Sea. *Biogeosciences*, *12*(3), 781–802. https://doi.org/10.5194/bg-12-781-2015
1356 Panassa, E., Santana-Casiano, J. M., González-Dávila, M., Hoppema, M., van Heuven, S. M.
1357 A. C., Völker, C., et al. (2018). Variability of nutrients and carbon dioxide in the
1358 Antarctic Intermediate Water between 1990 and 2014. *Ocean Dynamics*, *68*(3), 295–
1359 308. https://doi.org/10.1007/s10236-018-1131-2
1360 Park, G.-H., Lee, K., Tishchenko, P., Min, D.-H., Warner, M. J., Talley, L. D., et al. (2006).
1361 Large accumulation of anthropogenic CO2 in the East (Japan) Sea and its significant
1362 impact on carbonate chemistry. *Global Biogeochemical Cycles*, *20*(4).
1363 https://doi.org/10.1029/2005GB002676
1364 Patara, L., Böning, C. W., & Tanhua, T. (2021). Multidecadal Changes in Southern Ocean
1365 Ventilation since the 1960s Driven by Wind and Buoyancy Forcing. *Journal of*
1366 *Climate*, *34*(4), 1485–1502. https://doi.org/10.1175/JCLI-D-19-0947.1
1367 Perez, F. F., & Fraga, F. (1987). Association constant of fluoride and hydrogen ions in
1368 seawater. *Marine Chemistry*, *21*(2), 161–168. https://doi.org/10.1016/0304-
1369 4203(87)90036-3
1370 Pérez, F. F., Vázquez-Rodríguez, M., Mercier, H., Velo, A., Lherminier, P., & Ríos, A. F.
1371 (2010). Trends of anthropogenic CO_2 storage in North Atlantic water masses.
1372 *Biogeosciences*, *7*(5), 1789–1807. https://doi.org/10.5194/bg-7-1789-2010
1373 Pérez, Fiz F., Mercier, H., Vázquez-Rodríguez, M., Lherminier, P., Velo, A., Pardo, P. C., et

al. (2013). Atlantic Ocean CO2 uptake reduced by weakening of the meridional overturning circulation. *Nature Geoscience*, *6*(2), 146–152. https://doi.org/10.1038/ngeo1680

Poulter, B., Bastos, A., Canadell, J., Ciais, P., Gruber, N., Hauck, J., et al. (2022). Inventorying Earth's Land and Ocean Greenhouse Gases. *Eos*, *103*. https://doi.org/10.1029/2022eo179084

Raimondi, L., Tanhua, T., Azetsu-Scott, K., Yashayaev, I., & Wallace, D. w. r. (2021). A 30 - Year Time Series of Transient Tracer-Based Estimates of Anthropogenic Carbon in the Central Labrador Sea. *Journal of Geophysical Research: Oceans*, *126*(5), e2020JC017092. https://doi.org/10.1029/2020JC017092

Resplandy, L., Keeling, R. F., Rödenbeck, C., Stephens, B. B., Khatiwala, S., Rodgers, K. B., et al. (2018). Revision of global carbon fluxes based on a reassessment of oceanic and riverine carbon transport. *Nature Geoscience*, *11*(7), 504–509. https://doi.org/10.1038/s41561-018-0151-3

Ridge, S. M., & McKinley, G. A. (2021). Ocean carbon uptake under aggressive emission mitigation. *Biogeosciences*, *18*(8), 2711–2725. https://doi.org/10.5194/bg-18-2711-2021

Ríos, A. F., Velo, A., Pardo, P. C., Hoppema, M., & Pérez, F. F. (2012). An update of anthropogenic CO2 storage rates in the western South Atlantic basin and the role of Antarctic Bottom Water. *Journal of Marine Systems*, *94*, 197–203. https://doi.org/10.1016/j.jmarsys.2011.11.023

Sabine, C. L., Feely, R. A., Gruber, N., Key, R. M., Lee, K., Bullister, J. L., et al. (2004). The Oceanic Sink for Anthropogenic CO2. *Science*, *305*(5682), 367–371. https://doi.org/10.1126/science.1097403

Sallée, J.-B., Pellichero, V., Akhoudas, C., Pauthenet, E., Vignes, L., Schmidtko, S., et al.

(2021). Summertime increases in upper-ocean stratification and mixed-layer depth. *Nature*, *591*(7851), 592–598. https://doi.org/10.1038/s41586-021-03303-x

Sarmiento, J. L., & Gruber, N. (2006). *Ocean Biogeochemical Dynamics*. Princeton University Press.

Shi, J.-R., Talley, L. D., Xie, S.-P., Peng, Q., & Liu, W. (2021). Ocean warming and accelerating Southern Ocean zonal flow. *Nature Climate Change*, 1–8. https://doi.org/10.1038/s41558-021-01212-5

Sloyan, B. M., Wanninkhof, R., Kramp, M., Johnson, G. C., Talley, L. D., Tanhua, T., et al. (2019). The Global Ocean Ship-Based Hydrographic Investigations Program (GO-SHIP): A Platform for Integrated Multidisciplinary Ocean Science. *Frontiers in Marine Science*, *6*. https://doi.org/10.3389/fmars.2019.00445

Talley, L. d., Feely, R. a., Sloyan, B. m., Wanninkhof, R., Baringer, M. o., Bullister, J. l., et al. (2016). Changes in Ocean Heat, Carbon Content, and Ventilation: A Review of the First Decade of GO-SHIP Global Repeat Hydrography. *Annual Review of Marine Science*, *8*(1), 185–215. https://doi.org/10.1146/annurev-marine-052915-100829

Tanhua, T., Jones, E. P., Jeansson, E., Jutterström, S., Smethie, W. M., Wallace, D. W. R., & Anderson, L. G. (2009). Ventilation of the Arctic Ocean: Mean ages and inventories of anthropogenic CO2 and CFC-11. *Journal of Geophysical Research: Oceans*, *114*(C1). https://doi.org/10.1029/2008JC004868

Terhaar, J., Frölicher, T. L., & Joos, F. (2022). Observation-constrained estimates of the global ocean carbon sink from Earth system models. *Biogeosciences, 19*(18), 4431–4457. https://doi.org/10.5194/bg-19-4431-2022

Wallace, D. W. R. (1995). Monitoring Global Ocean Carbon Inventories.

Wanninkhof, R., Doney, S. C., Bullister, J. L., Levine, N. M., Warner, M., & Gruber, N. (2010). Detecting anthropogenic CO2 changes in the interior Atlantic Ocean between

1424 1989 and 2005. *Journal of Geophysical Research: Oceans*, *115*(C11).
1425 https://doi.org/10.1029/2010JC006251
1426 Watson, A. J., Schuster, U., Shutler, J. D., Holding, T., Ashton, I. G. C., Landschützer, P., et
1427 al. (2020). Revised estimates of ocean-atmosphere CO2 flux are consistent with ocean
1428 carbon inventory. *Nature Communications*, *11*(1), 4422.
1429 https://doi.org/10.1038/s41467-020-18203-3
1430 Weiss, R. F. (1970). The solubility of nitrogen, oxygen and argon in water and seawater.
1431 *Deep Sea Research and Oceanographic Abstracts*, *17*(4), 721–735.
1432 https://doi.org/10.1016/0011-7471(70)90037-9
1433 Woosley, R. J., Millero, F. J., & Wanninkhof, R. (2016). Rapid anthropogenic changes in
1434 CO2 and pH in the Atlantic Ocean: 2003–2014. *Global Biogeochemical Cycles*,
1435 *30*(1), 70–90. https://doi.org/10.1002/2015GB005248
1436 Yang, S., Gruber, N., Long, M. C., & Vogt, M. (2017). ENSO-Driven Variability of
1437 Denitrification and Suboxia in the Eastern Tropical Pacific Ocean. *Global*
1438 *Biogeochemical Cycles*, *31*(10), 1470–1487. https://doi.org/10.1002/2016GB005596
1439 Young, I. R., & Ribal, A. (2019). Multiplatform evaluation of global trends in wind speed
1440 and wave height. *Science*, *364*(6440), 548–552.
1441 https://doi.org/10.1126/science.aav9527
1442 Zweng, M. M., Reagan, J., Seidov, D., Boyer, T., Locarnini, R., Garcia, H., et al. (2019).
1443 *WORLD OCEAN ATLAS 2018 Volume 2: Salinity*.

References From the Supporting Information

Dlugokencky, E., & Tans, P. (2019). Trends in atmospheric carbon dioxide, National Oceanic & Atmospheric Administration, Earth System Research Laboratory (NOAA/ESRL). Retrieved from http://www.esrl.noaa.gov/gmd/ccgg/trends/global.html

Fong, M. B., & Dickson, A. G. (2019). Insights from GO-SHIP hydrography data into the thermodynamic consistency of CO2 system measurements in seawater. Marine Chemistry, 211, 52–63. https://doi.org/10.1016/j.marchem.2019.03.006

Garcia, H. E., Boyer, T., Baranova, O. K., Locarnini, R., Mishonov, A., Grodsky, A., et al. (2019). World Ocean Atlas 2018: Product Documentation. A. Mishonov, Technical Editor. Retrieved from https://www.ncei.noaa.gov/products/world-ocean-atlas

Jackett, D. R., & McDougall, T. J. (1997). A Neutral Density Variable for the World's Oceans. JOURNAL OF PHYSICAL OCEANOGRAPHY, 27, 27.

Johnson, K. M., Dickson, A. G., Eischeid, G., Goyet, C., Guenther, P., Key, R. M., et al. (1998). Coulometric total carbon dioxide analysis for marine studies: assessment of the quality of total inorganic carbon measurements made during the US Indian Ocean CO2 Survey 1994–1996. Marine Chemistry, 63(1), 21–37. https://doi.org/10.1016/S0304-4203(98)00048-6

Johnson, K. M., Dickson, A. G., Eischeid, G., Goyet, C., Guenther, P. R., Key, R. M., et al. (2002). Carbon Dioxide, Hydrographic and Chemical Data Obtained During the Nine R/V Knorr Cruises Comprising the Indian Ocean CO2 Survey (WOCE Sections I8SI9S, I9N, I8NI5E, I3, I5WI4, I7N, I1, I10, and I2, and 12; December 1, I994-January 22, 1996) [Data set]. NOAA National Centers for Environmental Information. https://doi.org/10.3334/CDIAC/OTG.NDP080

Murata, A., Kumamoto, Y., Sasaki, K., Watanabe, S., & Fukasawa, M. (2010). Decadal

increases in anthropogenic CO2 along 20°S in the South Indian Ocean. Journal of Geophysical Research: Oceans, 115(C12). https://doi.org/10.1029/2010JC006250

Olsen, A., Lange, N., Key, R. M., Tanhua, T., Álvarez, M., Becker, S., et al. (2019). GLODAPv2.2019 – an update of GLODAPv2. Earth System Science Data, 11(3), 1437–1461. https://doi.org/10.5194/essd-11-1437-2019

Sabine, C. L., Key, R. M., Johnson, K. M., Millero, F. J., Poisson, A., Sarmiento, J. L., et al. (1999). Anthropogenic CO2 inventory of the Indian Ocean. Global Biogeochemical Cycles, 13(1), 179–198. https://doi.org/10.1029/1998GB900022

Sharp, J. D., & Byrne, R. H. (2020). Interpreting measurements of total alkalinity in marine and estuarine waters in the presence of proton-binding organic matter. Deep Sea Research Part I: Oceanographic Research Papers, 165, 103338. https://doi.org/10.1016/j.dsr.2020.103338

Tsujino, H., Urakawa, S., Nakano, H., Small, R. J., Kim, W. M., Yeager, S. G., et al. (2018). JRA-55 based surface dataset for driving ocean–sea-ice models (JRA55-do). Ocean Modelling, 130, 79–139. https://doi.org/10.1016/j.ocemod.2018.07.002